Science of The Total Environment
April 2022, Volume 818, Pages 151680 (24p.)
https://doi.org/10.1016/j.scitotenv.2021.151680
https://archimer.ifremer.fr/doc/00735/84659/

Metal stresses modify soluble proteomes and toxin profiles in two Mediterranean strains of the distributed dinoflagellate *Alexandrium pacificum*

Jean Natacha [1, *], Perié Luce [2], Dumont Estelle [3], Bertheau Lucie [5], Balliau Thierry [4], Caruana Amandine [6], Amzil Zouher [6], Laabir Mohamed [7], Masseret Estelle [7]

[1] Université de Toulon, Aix Marseille Univ, CNRS, IRD, MIO, Toulon, France
[2] Division of Endocrinology, Diabetes and Metabolism, Department of Medicine, New York University, 30th St., New York, NY 10016, USA
[3] UMR_MD1, Aix-Marseille Univ, U-1261-INSERM, SSA, IRBA, MCT, Marseille, France
[4] PAPPSO-GQE-Le Moulon, INRA, Université Paris-Sud, CNRS, AgroParisTech, Université Paris-Saclay, 91 190 Gif-sur-Yvette, France
[5] UMR PAM A 02.102 Procédés Alimentaires et Microbiologiques, Université de Bourgogne Franche-Comté, AgroSup Dijon, esplanade Erasme, 21 000 Dijon, France
[6] IFREMER, Phycotoxin Laboratory, rue de l'île d'Yeu, BP 21105, 44 311 Nantes, France
[7] Marbec, Univ Montpellier, IRD, Ifremer, CNRS, Montpellier, France

* Corresponding author : Natacha Jean, email address : natacha.jean@mio.osupytheas.fr

Abstract :

HABs involving Alexandrium pacificum have been reported in metal-contaminated ecosystems, suggesting that this distributed species adapts to and/or can tolerate the effects of metals. Modifications in soluble proteomes and PST contents were characterized in two Mediterranean A. pacificum strains exposed to mono- or polymetallic stresses (zinc, lead, copper, cadmium). These strains were isolated from two anthropized locations: Santa Giusta Lagoon (Italy, SG C10–3) and the Tarragona seaport (Spain, TAR C54F). In both strains, metals primarily downregulated key photosynthesis proteins. Metals also upregulated other proteins involved in photosynthesis (PCP in both strains), the oxidative stress response (HSP 60, proteasome and SOD in SG C10–3; HSP 70 in TAR C54F), energy metabolism (AdK in TAR C54F), neoglucogenesis/glycolysis (GAPDH and PEP synthase in SG C10–3) and protein modification (PP in TAR C54F). These proteins, possibly involved in adaptive proteomic responses, may explain the development of these A. pacificum strains in metal-contaminated ecosystems. The two strains showed different proteomic responses to metals, with SG C10–3 upregulating more proteins, particularly PCP. Among the PSTs, regardless of the metal and the strain studied, C2 and GTX4 predominated, followed by GTX5. Under the polymetallic cocktail, (i) total PSTs, C2 and GTX4 reached the highest levels in SG C10–3 only, and (ii) total PSTs, C2, GTX5 and neoSTX were higher in SG C10–3 than in TAR C54F, whereas in SG C10–3 under copper stress, total PSTs, GTX5, GTX1 and C1 were higher than in the controls, revealing variability in PST biosynthesis between the two strains. Total PSTs, C2, GTX4 and GTX1 showed significant positive correlations with PCP, indicating that PST production may be positively related to photosynthesis. Our results showed that the A. pacificum strains adapt their proteomic and physiological responses to metals, which may contribute to their ecological success in highly anthropized areas.

Graphical abstract

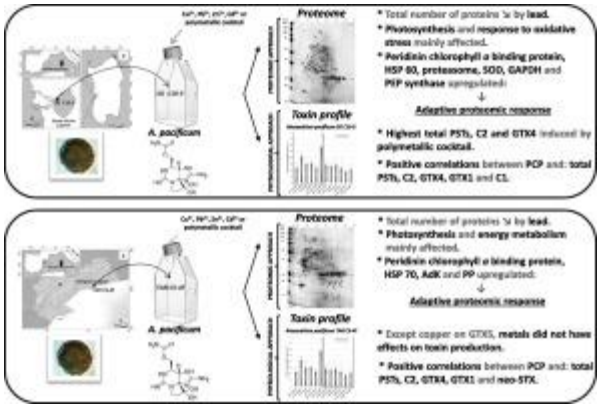

Highlights

► Metals modify soluble proteomes and toxin profiles in the *A. pacificum* strains. ► Downregulation of photosynthesis proteins was observed in the *A. pacificum* strains exposed to metals. ► Adaptive proteomic response exist in the *A. pacificum* strains under metal stress conditions. ► SG C10–3 strain upregulates more proteins than TAR C5—4F strain, revealing proteomic variability between the two strains exposed to metals. ► Polymetallic cocktail and copper have significant effects on the PST contents in the SG C10–3 strain. ► PST showed correlations with PCP in both strains: photosynthesis may be positively related to toxin production.

Keywords : Alexandrium pacificum, harmful algal bloom, paralytic shellfish toxin, proteomics, metal

Abbreviations

ACN	Acetonitrile
AdK	Adenosine kinase
ADSS	Adenylosuccinate synthetase
AGMAT	Agmatinase
CALR	Calreticulin
CHAPS	3-[3-(cholamidopropyl)-dimethylammonio]1-propanesulfonate
2-DE	Two-dimensional gel electrophoresis
DTT	Dithiothreitol
FNR	Chloroplast ferredoxin-NADP(+) reductase
GAPDH	Glyceraldehyde-3-phosphate dehydrogenase
GTX	Gonyautoxin
HAB	Harmful algal bloom
HSP	Heat shock protein
IEF	Isoelectric focusing
IPG	Immobilized pH gradient
Kat	Catalase peroxidase
LAP	Leucine aminopeptidase
LBP	Luciferin-binding protein
LC-MS/MS	Liquid chromatography coupled to tandem mass spectrometry
MAT	Methionine S-adenosyl transferase
MS	Mass spectrometry
MS/MS	Tandem mass spectrometry
MW	Molecular weight
NCBI	National Center for Biotechnology Information
NRC	National Research Council
PCOX	Post-column oxidation method
PCP	Peridinin chlorophyll *a* binding protein
PEP	Protein expression profile
PEP synthase	Phosphoenolpyruvate synthase
pI	Isoelectric point
PKC	Protein kinase C
PP	Serine/threonine-protein phosphatase
PSP	Paralytic shellfish poisoning
PST	Paralytic shellfish toxin
ROS	Reactive oxygen species
RPI	Ribose-5-phosphate isomerase
RUBISCO	Ribulose bisphosphate carboxylase
SCP	Serine carboxypeptidase
SDS	Sodium dodecylsulfate
SDS-PAGE	Sodium dodecylsulfate-polyacrylamide gel electrophoresis
SOD	Copper/zinc superoxide dismutase
STX	Saxitoxin

Introduction

The marine dinoflagellate *Alexandrium*, involved in harmful algal blooms (HABs), can produce the neurotoxic alkaloids called saxitoxins (STXs) that induce the paralytic shellfish poisoning (PSP) syndrome (Anderson et al., 2012). STXs, which are paralytic shellfish toxins (PSTs), are tetrahydropurine neurotoxins that are active on voltage-gated sodium channels of excitable cells (Kao and Walker, 1982). They cause (*i*) human neural system syndromes (Quod and Turquet, 1996), (*ii*) mass mortalities of fish, shellfish, marine mammals and birds (Hallegraeff, 1993), and (*iii*) high economic losses for aquaculture or shellfish farming (Hoagland et al., 2002; Park et al., 2013). Toxin profiles and concentrations in *Alexandrium* STX producers may differ at interspecific (Caruana et al., 2010) and intraspecific levels (Hadjadji et al., 2020). The biological roles of STXs are not fully understood, although increased STX production in *Alexandrium minutum* cells cultivated in presence of the copepod *Acartia tonsa* suggests that STXs may protect this species against grazers (Selander et al., 2006). Increased Cu^{2+} levels stimulated STX production in cyanobacteria and in microalgae, as observed for example in the cyanobacterium *Raphidiopsis raciborskii*, and STXs could bind to metal transporters in microorganisms, consequently alleviating metal stress (Giraldi et al., 2021).

Alexandrium pacificum Litaker [ex *A. catenella* (Whedon and Kofoid), Balech], once considered as a rare species in the Mediterranean Sea (Margalef and Estrada, 1987), is now widely distributed. It forms blooms in the metal-contaminated Annaba Bay (Algeria), along the Tyrrhenian coasts of Italy, the Balearic and Catalonian coasts of Spain, Thau Lagoon (France) and Bizerte Lagoon (Tunisia) (Bravo et al., 2008; Fertouna-Bellakhal et al., 2015; Hadjadji et al., 2020; Laabir et al., 2013; Penna et al., 2005), which suggests that it can adapt and/or is tolerant to metal contamination. *Alexandrium* spp. are also observed in Toulon Bay (western Mediterranean Sea, France), where the water column and sediments are severely metal-contaminated (Jean et al., 2005, 2012; Tessier et al., 2011).

Omics approaches are powerful tools for revealing the responses and the adaptation mechanisms that organisms exposed to environmental stresses have developed (Jean et al., 2012). Proteomic studies have been carried out to better understand *A. pacificum* toxin biosynthesis and its stages (Wang et al., 2013; Zhang et al., 2015). However, few studies have investigated the ability of *A. pacificum* to adapt to and/or tolerate disturbed environments such as metal-contaminated coastal ecosystems. *In silico* prediction of the *A. pacificum* secretome, outside specific conditions, has shown that proteins released in the extracellular medium are

mainly enzymes (Chetouhi et al., 2019). Enzymatic activity of these secreted proteins could contribute to regulate the extracellular environment and be involved in some stress responses, which may help this dinoflagellate to develop in metal-contaminated conditions. A proteomic study on the Mediterranean *A. pacificum* strain ACT03 (isolated from Thau Lagoon, France) exposed to monometallic stresses revealed upregulated proteins (ATP synthase) that contribute to an adaptive proteomic response of this dinoflagellate in metal-contaminated ecosystems (Jean et al., 2017). Chetouhi et al. (2020) have combined ecotoxicoproteomic (membrane proteomes) and physiological (morphometry) approaches to compare the responses to polymetallic stress (zinc, lead, copper and cadmium used in cocktail) of the Mediterranean *A. pacificum* strains SG C10-3 and TAR C5-4F, respectively coming from the metal-contaminated Mediterranean areas of the Santa Giusta Lagoon (Luglié et al., 2002) and the Tarragona seaport (Bravo et al., 2008). In these conditions, the strains showed differences in cell growth and morphometry, in addition to different modifications of the membrane proteomes, potentially conferring to the ability for adaptation and/or tolerance under metal stresses. The present study aims to extend the proteomic and physiological data obtained for these *A. pacificum* strains (*i*) to assess the variation in their PST production and (*ii*) to determine the modifications of their soluble proteomes under different metal stresses (zinc, lead, copper, cadmium: used in cocktail or single). Based on the responses observed, we investigate how these *A. pacificum* strains modulate their toxin production and their soluble proteome to enhance their tolerance in metal-contaminated ecosystems.

Materials and methods

1. Alexandrium pacificum cultures

1.1. Strains

The two strains of *Alexandrium pacificum* were obtained from the germination of single cysts isolated from sediments collected respectively in the Santa Giusta Lagoon (Sardinia, Italy) for the SG C10-3 strain and in the Tarragona seaport (Spain) for the TAR C5-4F strain (**Figure 1**). They were genotyped with microsatellites markers for an on-going population genetic analysis showing they are *A. pacificum* (unpublished data). Metal contamination has been reported in the surface sediments of the Santa Giusta Lagoon (Zn^{2+}=47.6 µg g^{-1}, Pb^{2+}=9.9 µg g^{-1}, Cu^{2+}=9.6 µg g^{-1} and Cd^{2+}=3.8 µg g^{-1}) (Luglié et al., 2002). The shallow sediments of the Tarragona seaport, an area of intense shipping traffic that receives discharges from major rivers, are also metal contaminated (Zn^{2+}=45.0 µg g^{-1}, Pb^{2+}=19.9 µg g^{-1}, Cu^{2+}=12.1 µg g^{-1} and Cd^{2+}=0.6 µg g^{-1}) (Bravo et al., 2008; Pinedo et al., 2014). Considering previous works (Laabir

et al., 2011, 2013; Jean et al., 2017), the growth kinetics, the toxin profiles and the metabolic functions impacted by metals through modifications of the respective proteomes in SG C10-3 and in TAR C5-4F are close to those of *A. pacificum* ACT03 strain, which has been widely studied and could be considered as a reference strain.

1.2. Cultures

The obtained monoclonal cultures of these two strains were maintained in f/2 culture medium (*i.e.* containing: $NaNO_3$, NaH_2PO_4, Na_2EDTA, $FeCl_3$, $ZnSO_4$, $CoSO_4$, $MnSO_4$, Na_2MoO_4, Na_2SeO_3, $NiCl_2$, thiamine HCl, biotin, cyanocobalamin) (Guillard and Ryther, 1962) at 20°C, in sterile 250 mL flasks (75 cm^2 Greiner, Dominique Dutscher SAS), under a light intensity of 135 µmol photons m^{-2} s^{-1}, with a photoperiod of L12:D12 (light:dark) (Herzi et al., 2013, 2014). Natural seawater, filtered through a GF/F grade glass fiber filter (Ø= 47 mm, Whatman) and then sterilized, was used for preparing the culture medium.

To study the variability in the soluble proteomes and PSTs of *A. pacificum* cultures under metal stress conditions, the f/2 medium was supplemented with, either (*i*) a monometallic sterile stock solution prepared with a metal salt (either $ZnSO_4,7H_2O$, or $Pb(CH_3COO)_2,3H_2O$, or $CuSO_4,2H_2O$, or $3CdSO_4,8H_2O$: chosen for their solubility) dissolved in ultrapure water to reach a concentration of 6 µM in the culture medium, or (*ii*) a polymetallic cocktail, obtained from the monometallic sterile stock solutions, with 6 µM total concentration in the culture medium (meaning that Zn^{2+}, and Pb^{2+}, and Cu^{2+}, and Cd^{2+} were at a concentration of 1.5 µM in this medium) (**Figure 2A**). Metal-free culture medium was used as control. Trace metals used in this study have been chosen since they frequently contamine marine metal-contaminated coastal ecosystems: Zn^{2+} and Cu^{2+} are essential for cells as oligo-elements but toxic at high levels, whereas Pb^{2+} and Cd^{2+} are always toxic for the cells (Tripathi and Poluri, 2021). Based on the MINEQL program (Garnier et al., 2004) and on the known composition of the f/2 medium, the estimated corresponding bioavailable toxic free metal (M_F^{2+}) concentrations were calculated (Herzi et al., 2013, 2014): $Zn_F^{2+} = 0.67 \times 10^{-7}$ M, $Pb_F^{2+} = 2.56 \times 10^{-9}$ M, $Cu_F^{2+} = 4.96 \times 10^{-10}$ M, $Cd_F^{2+} = 0.70 \times 10^{-8}$ M. Previous studies showed impact of these concentrations on *A. pacificum* growth kinetics (Herzi et al., 2013, 2014), besides they are similar to those usually measured in marine metal contaminated coastal ecosystems (Jean et al., 2012; Tessier et al., 2011). Preliminary kinetics experiments showed that growth phase may influence the proteomic response of the *A. pacificum* cells exposed to metals (article in preparation). The data obtained showed that 15 days of exposure led to the most important changes in the *A. pacificum* soluble proteome. Consequently, in the present study, the *A.*

pacificum cells were exposed to metals during the first 15 days of growth, so as to observe variability of the dinoflagellate proteomic responses in the tested metal-contaminated conditions. To analyze the soluble proteomes and PST contents, three independent biological replicates of the SG C10-3 and TAR C5-4F *A. pacificum* cultures were used for the controls and in each metal stress condition.

1.3. PST measurements

For each condition described above (control or metal-stressed), PST measurements were carried out on aliquots of the corresponding SG C10-3 and TAR C5-4F *A. pacificum* cultures at the end of the exponential phase-early stationary phase of their growth (after 15 days of growth), systematically containing 1.8×10^6 cells resuspended in acetic acid (0.1 N) and frozen at -20°C until analysis (**Figure 2B**). Cell densities of the cultures were estimated by counting (in triplicate) all the cells contained in 50 µL subsample of a 1 mL Lugol-fixed culture sample, under an inverted microscope (magnification: 100×).

To release toxins, cells were lysed by grinding with 250 mg glass beads (150 µm, VWR, France) in a mixer mill (Retsch MM400, Haan, Germany) for 30 min at 30 Hz. Then, lysates were centrifuged (17 000 g, 10 min, °C centrifuge 3–18K, Sigma, Osterode am Harz, Germany) and supernatants filtered through a 0.2 µm inert filter (Nanosep, Pall, Saint-Germain-en-Laye, France). Samples were then analyzed or stored at -20°C until analyses. Toxin analyses were based on the post-column oxidation method (PCOX) (Van de Riet et al., 2009) and was performed using the LC/FLD Agilent 1200 series analytical system (Agilent Technologies, Massy, France). Two groups of toxins were separated using reversed-phase chromatography with two different columns. A C_{18} column (Zorbax Bonus RP, 150×4.6 mm, 3.5 µm) was filled with a step gradient of a heptane sulfonic acid/phosphoric acid buffer system and acetonitrile (ACN) for the analysis of GTXs, dc-GTXs, dc-STXs and STX. A C_8 column (BetaBasic, 8.5 µm, 250×4.6 mm) with an isocratic tetrabutylammonium phosphate buffer system and ACN was used for the C toxins. A derivation of toxins was carried out using PCOX with a phosphoric acid/periodic acid buffer solution at 85°C. This oxidized eluent was acidified using nitric acid, and the derivatives were detected using fluorescence (excitation: 330 nm, emission: 395 nm). Toxin concentrations were calculated based on standard curves constructed from certified reference standards obtained from the NRC (Halifax, Nova Scotia, Canada).

1.4. Statistical analysis

Student's *t*-tests were used to compare the means of PST contents, the means of total number of protein spots, in the control and in each metal stress condition, for the three independent biological replicates of the SG C10-3 or the TAR C5-4F *A. pacificum* cultures (Shapiro-Wilk's test showed that the data followed a normal distribution: $P > 0.05$).

As used by Savela et al. (2016) to correlate quantity of the STXA4 gene and cell density with PST production in *Alexandrium ostenfeldii*, we used Spearman's rank correlation coefficients to detect the significant (positive or negative) correlations (*i*) between the various PST contents and (*ii*) between PST contents and protein spot abundances, under control and metal stress conditions.

2. Proteomic analysis and protein identification using mass spectrometry

Proteomic analyses were carried out on samples coming from three independent biological replicates of the SG C10-3 or TAR C5-4F *A. pacificum* cultures (the same replicates as those used for PST measurements) at the end of the exponential phase-early stationary phase of their growth (after 15 days of growth), in control and in metal contaminated conditions (**Figure 2C**). A culture sample containing 8×10^6 cells was systematically used for one proteomic analysis/replicate.

2.1. Preparation of protein extracts

The culture sample was centrifuged for 15 min at 1 500 g at 15°C. The obtained cell pellet was washed twice with sterile filtered natural seawater for 10 min at 15 000 g (Wang et al., 2008). The pellet was then re-suspended in extraction solution containing 2 mL of 40 mM Tris at pH 8.7, 2.4 µL benzonase nuclease (Sigma-Aldrich), and 10 µL of protease inhibitor cocktail (Sigma-Aldrich). The obtained suspension was sonicated in an ice-water bath, using a microtip Vibra Cell 734 24 (Bioblock Scientific) for 3 min (10 s on/10 s off cycles) at 50 W and 25 kHz. Then, solution was centrifuged for 30 min at 15 000 g. The obtained supernatant was concentrated by ultrafiltration (at 1 500 g and 15°C) through Vivaspin concentrator tubes (molecular weight cutoff membranes of 10 kDa, 15R Hydrosart 10 kDa, Thermo Fisher Scientific) until reaching 150 µL concentrate. The protein extract was obtained by mixing this concentrate with 400 µL of sample solution containing 7 M urea, 2 M thiourea, 1 % w/v CHAPS, 3 % v/v Triton X-100, 1 % w/v DTT, 0.2 % v/v carrier ampholytes and 0.002 % v/v bromophenol blue.

2.2. Protein determination

Protein determination of the protein extracts was achieved using the Reagent Compatible Detergent Compatible Protein Assay (RC DC Protein Assay, Bio-Rad) based on the Lowry method (Lowry et al., 1951), with bovine serum albumin (BSA) as standard.

2.3.2-D electrophoresis

According to Rabilloud and Lelong (2021), 2-DE is a still highly valuable tool especially when quantitative comparisons of samples must be made, and even for large samples series. 2-DE still offers unique advantages that make it stand apart (and ahead) of the other proteomic setups. Besides, 2-DE is the simplest technique that is able to resolve complete proteins with their trail and combination of post-translational modifications, including protein fragmentation, and this unique ability should be highly valued with our increased knowledge on the importance of post-translational modifications on protein activity. Thus, 2D gel-based proteomics has still a lot to offer to the researchers who will be able to use its strengths. Here, 2-DE was performed using 350 µL of extract containing 200 µg of proteins loaded on a preprepared immobilized pH gradient (IPG) strip (17 cm length, linear gradient, pH 3–10, Bio-Rad) (Linares et al., 2016). Rehydration and then isoelectric focusing (IEF) of the extract within the IPG strip, was performed using a Protean IEF Cell (Bio-Rad) horizontal electrophoresis system at 20°C. The IEF program used was as follows: 18 h at 50 V (active rehydration), 2 h at 100 V, 2 h at 250 V, 2 h at 500 V, 2 h at 1 000 V, 2 h at 4 000 V and 5 h at 10 000 V, to reach 60 000 Vh for each loaded IPG strip. After IEF, the equilibration of each IPG strip was performed for 10 min at room temperature, in equilibration buffer 1 (6 M urea, 2 % w/v SDS, 0.375 M Tris pH 8.8, 20 % v/v glycerol and 2 % w/v DTT), and then, in equilibration buffer 2 (6 M urea, 2 % w/v SDS, 0.375 M Tris pH 8.8, 20 % v/v glycerol and 2.5 % w/v iodoacetamide). The proteins separated by IEF underwent SDS-PAGE (Laemmli, 1970) in 18-cm 12 % polyacrylamide gels (strip was positioned at the top of the polyacrylamide gels and sealed with 0.7 % agarose). A volume of 20 µL of a molecular weight marker solution (10–250 kDa range, Precision Plus Protein Standards Dual Color, Bio-Rad) was loaded at the top left-hand corner of the gel. The gels were run at 4°C in a Protean II XL Cell (Bio-Rad), with a constant current of 20 mA per gel for 1 h and then with a constant current of 30 mA per gel until the dye reached the bottom of the gel. At the end of SDS-PAGE, gels were washed three times for 5 min in ultrapure water, then stained with the Imperial Protein Stain (Thermo Fisher Scientific) under orbital shaking for 1.5 h. The stained gels were destained in ultrapure water until visualization of separated protein spots. Each gel shown in this study was a good representative of the three biological

(gel) replicates. The protein spots on the gels were analyzed using PD-Quest 2-D Analysis Software 8.0.1 (Bio-Rad). The abundance of a protein spot was obtained, after normalization, based on the *ratio* (in %) of its individual abundance to the abundance of all the standard marker bands.

2.4. Tracking of differentially expressed proteins

A protein of interest was defined as a significantly differentially expressed protein in response to a given metal stress, either by significant upregulation (or appearance) of the corresponding spots on the contaminated 2-D gels relative to those of controls, or by significant downregulation (or disappearance) of the corresponding spots on the control 2-D gels relative to those obtained in the metal stress condition (Jean et al. 2017). To be considered as potentially upregulated, the protein considered had to show a *ratio* of ≥ 2 of the normalized abundance of its spot on the contaminated 2-D gels relative to the normalized abundance of this spot on the control 2-D gels (Bae et al., 2003). Similarly, to be regarded as potentially downregulated, the protein had to show a *ratio* of ≤ 2 of the normalized abundance of its spot on the contaminated 2-D gels relative to the normalized abundance of this spot on the control 2-D gels. Then, to finalize this determination, abundances of the corresponding spots on the control and on the metal-contaminated 2-D gels were compared using a Student's *t*-test. If the Student's *t*-test showed significant differences in these abundances (highly significant: $P^{***} \leq 0.01$; significant: $0.01 < P^{**} \leq 0.05$, nearly significant: $0.05 < P^{*} \leq 0.10$), the corresponding spot was considered be composed of a up- or downregulated protein of interest. Significantly appeared/disappeared proteins corresponded to spots respectively appearing/disappearing on at least two of the three metal contaminated gel replicates, in comparison with controls.

2.5. Protein identification using liquid chromatography-tandem mass spectrometry

To identify a protein of interest by liquid chromatography-tandem mass spectrometry (LC-MS/MS), the corresponding spot was excised from gel replicates. Protein digestion of the excised spots was carried out according to a standard trypsin protocol (Aloui et al., 2018). An Ultimate 3000 RSLC nano system (Thermo Scientific) was used for HPLC. A volume of a 4 µL solution containing the peptide sample was loaded at 30 µL min^{-1} on a precolumn cartridge (stationary phase: C18 PepMap, 5 µm; column: 300 µm inner diameter, 5 mm; Thermo Scientific) and desalted with 0.08 % trifluoroacetic acid and 2 % ACN in water.

Three minutes later, the precolumn cartridge was connected to the separating PepMap C18 column (stationary phase: C18 PepMap, 3 μm; column: 75 μm inner diameter, 150 mm; Thermo Scientific). Buffer A was prepared with 0.1 % HCOOH and 3 % ACN in water, and buffer B with 0.1 % HCOOH and 80 % ACN in water. The peptides were separated using a linear gradient from 4 to 39 % B for 14 min at μL min^{-1}. Including the regeneration step at 99 % B and the equilibration step at 4 % A, one run took 22 min. LTQ Orbitrap Discovery (Thermo Electron) was used to analyze the eluted peptides using a nanoelectrospray interface. Liquid junction and a non-coated capillary probe (10 μm inner diameter; New Objective) were used for ionization (1.4 kV ionization potential). Peptide ions were analyzed using Xcalibur 2.5.5 SP1 with the following data-dependent acquisition steps: (1) full MS scan (mass-to-charge *ratio* (*m*/*z*) 300 -1 400, centroid mode in orbitrap) and (2) MS/MS (qz = 0.22, activation time = 50 ms, and collision energy = 35 %; centroid mode in linear trap). Step 2 was repeated for the three major ions detected in step 1. Dynamic exclusion was set to 30 s. Database searches were carried out using X!Tandem (Craig and Beavis, 2004). For protein identification, the *A. pacificum* database from Zhang et al. (2014) (11 437 entries) and a common contaminant database (keratins, trypsin, etc.: 55 entries) were used. Protein identification was parsed/validated using the X!TandemPipeline tool when at least two peptides (at 0.05 E-value) originating from a single protein (at 0.001 E-value) were significant (Langella et al., 2017). Not all the proteins of the proteomes could be identified in cases where: (*i*) the corresponding spots were too small (thus impossible to excise from the gels), (*ii*) the proteins could not be sequenced for other technical reasons or (*iii*) the corresponding protein sequences remained unknown (or hypothetical) in the proteomic databases.

Results

1. Effects of metals on the soluble proteomes of the A. pacificum *strains*

1.1. Effects of metals on the soluble proteome of *A. pacificum* SG C10-3

LC-MS/MS identification and functional annotations for the proteins modified in expression (= proteins of interest) in the SG C10-3 strain are shown in **Table 1**.

1.1.1. Effects of copper contamination

The protein expression profile (PEP) obtained for the SG C10-3 cells exposed to copper showed 362 ± 27 spots (**Figure 3A**). This was not significantly different (Student's *t*-test: P > 0.10) from controls (346 ± 89 spots).

27 % of the expressed soluble proteome varied in response to copper, with 17 % proteins significantly downregulated or disappeared, and 10 % proteins appeared (**Figure 3B)**. The appeared proteins included proteasome subunit (spot 209), HSP 60 (spot 177) and PEP synthase (spot 207), whereas downregulated or disappeared proteins included SCP (spots 16 and 194) and SOD (spot 48). Contrasting effects of copper (appearance and disappearance of different spots of the same protein) were observed for GAPDH (spots 131, 212 and 217), FNR (spots 40, 110, 114 and 211) and PCP (spots 170, 171, 205 and 210).

Proteins of interest were primarily assigned to (**Figure 4**): first, photosynthesis (20 % of proteins of interest) with contrasting expression of FNR and PCP, then, the oxidative stress response (10 % of proteins of interest) with upregulated proteasome subunit and HSP 60, but downregulated SOD. The other affected functions were: energy metabolism and protein degradation (8 %, contrasting expression of FNR and downregulated SCP, respectively), neoglucogenesis (6 %, upregulated PEP synthase and contrasting GAPDH), glycolysis (4 %, contrasting effects on GAPDH) and chaperone activity (2 %, upregulated HSP 60).

1.1.2. Effects of lead contamination

In response to lead stress, the PEP showed 211 ± 58 spots, which was significantly lower than the controls by 39 % (Student's *t*-test: $0.01 < P^{**} \leq 0.05$) (**Figure 3A**).

37 % proteins were differently expressed under lead stress: 28 % proteins were downregulated or disappeared, and 9 % proteins were upregulated or appeared (**Figure 3B**). The upregulated or appeared protein was PCP (spots 78, 170 and 171), whereas downregulated or disappeared proteins were FNR (spot 110), RUBISCO (spots 47 and 107) and Kat (spot 77). Contrasting effects of lead were observed for SOD (spot 48 downregulated, but spot 175 appeared) and HSP 60 (spot 74 downregulated, but spot 177 appeared).

Two main functions involved these proteins of interest (**Figure 4**): photosynthesis (25 % of proteins of interest) with upregulated PCP and downregulated RUBISCO and FNR, and the oxidative stress response (22 % of proteins of interest) with SOD and HSP 60, and downregulated Kat. The other functions were: chaperone activity (6 %, with contrasting effects on HSP 60), photorespiration (6 %, with downregulated RUBISCO) and energy metabolism (3 %, with downregulated FNR).

1.1.3. Effects of zinc contamination

Zinc stress led to 344 ± 47 spots (**Figure 3A**). This was not significantly different (Student's *t*-test: $P > 0.10$) from controls.

23 % of the soluble proteome showed modified expression in response to zinc: 15 % proteins were downregulated or disappeared, and 8 % proteins were upregulated or appeared (**Figure 3B**). Upregulated or appeared proteins included PCP (spots 126, 170, 171, 187 and 210) and HSP 60 (spot 177), whereas downregulated or disappeared proteins included GAPDH (spot 131), FNR (spots 61 and 114), RUBISCO (spot 119), Kat (spot 77) and AdK (spot 124). Zinc stress resulted in antagonistic effects for SOD (spots 48 downregulated, but spot 175 appeared).

First, photosynthesis was the main function affected (29 % of proteins of interest) with contrasting effects on PCP and downregulated RUBISCO and FNR. Then, it was the oxidative stress response (15 % of proteins of interest) with upregulated HSP 60, contrasting effects on SOD and downregulated Kat. Energy metabolism (9 %, with downregulated FNR and AdK), photorespiration (2 %, with downregulated RUBISCO), chaperone activity (2 %, with upregulated HSP 60) and neoglucogenesis/glycolysis (2 %, with downregulated GAPDH) were also impacted.

1.1.4. Effects of cadmium contamination

Under cadmium stress, 421 ± 81 spots were found, which was not significantly different (Student's *t*-test: P > 0.10) from controls (**Figure 3A**).

14 % of proteins were modified in expression in response to cadmium: 8 % proteins were downregulated or disappeared, and 6 % proteins were upregulated or appeared (**Figure 3B**). Among the downregulated or disappeared proteins, were: GAPDH (spot 131), FNR (spot 110), RUBISCO (spot 119), proteasome subunit (spots 140 and 147), Kat (spot 77), ATP synthase (spot 139) and CO_2 inducible protein (spot 52). Contrasting effects of cadmium (upregulation/appearance or downregulation for different spots of the same protein) were observed for PCP (spots 126, 141 and 142) and HSP 60 (spots 74 and 177).

Proteins of interest were mainly assigned to (**Figure 4**): first, the oxidative stress response (27 % of proteins of interest) with contrasting effects on PCP and downregulated RUBISCO, FNR and ATP synthase, and photosynthesis (24 % of proteins of interest) with downregulated Kat, CO_2 inducible protein, proteasome subunit and HSP 60. The other functions included chaperone activity (6 %, downregulated HSP 60), photorespiration (3 %, downregulated RUBISCO), energy metabolism (3 %, downregulated FNR and ATP synthase) and neoglucogenesis/glycolysis (3 %, downregulated GAPDH).

1.1.5. Effects of cocktail

In response to polymetallic cocktail stress, the PEP showed 306 ± 93 spots (**Figure 3A**). This was not significantly different (Student's *t*-test: P > 0.10) from controls.

27 % of proteins of interest were found: 21 % proteins were downregulated or disappeared, and 6 % proteins were upregulated or appeared (**Figure 3B**). Among upregulated or appeared proteins, we observed PCP (spots 68, 170, 171, 186, 187 and 210) and proteasome subunit (spot 209), whereas downregulated or disappeared proteins included GAPDH (spot 1), SCP (spot 16), FNR (spots 40, 61 and 62), RUBISCO (spot 47), SOD (spot 48) and CO_2 inducible protein (spot 52).

Polymetallic cocktail induced proteins of interest mainly assigned to (**Figure 4**): photosynthesis (35 % of proteins of interest) with upregulated PCP and downregulated RUBISCO and FNR, and oxidative stress response (13 % of proteins of interest) with upregulated proteasome subunit and downregulated SOD and CO_2 inducible protein. Other functions included energy metabolism (7 %, downregulated FNR), protein degradation (4 %, downregulated SCP), neoglucogenesis and glycolysis (2 %, downregulated GAPDH) and photorespiration (2 %, downregulated RUBISCO).

1.1.6. Comparison of the proteomic modifications under the different metal stresses

Lead significantly reduced (by 39 %) the total number of proteins and the other metals had no significant effect. Lead contamination led to the most important quantitative proteomic modifications (37 %), whereas cadmium had the lowest impact on them (14 % proteins with modified expression). Lead induced the highest proportion of downregulated or disappeared proteins (28 %), in comparison with the other metals, followed by the polymetallic cocktail (21 %), copper (17 %), zinc (15 %) and cadmium (8 %). Metals induced similar proportions of upregulated or appeared proteins, ranging from 10 % proteins in response to copper to 6 % proteins in response to cadmium.

Regardless of the metal stress, photosynthesis was the most affected, through the upregulation of PCP, associated with the downregulation of FNR/RUBISCO (except with copper) and occasionally with downregulated ATP synthase (with cadmium). Photosynthesis was the most impacted by polymetallic stress (35 % of proteins involved), but copper affected it the least (20 % of proteins involved were differentially expressed under copper stress). Then, it was the oxidative stress response (cadmium impacted the most), through the upregulation of HSP 60 (with copper, lead, zinc and cadmium) and/or proteasome subunit (with copper and the polymetallic cocktail), rarer downregulation of these proteins in response to lead or cadmium, occasional upregulation of SOD (with lead and zinc), downregulation of SOD and/or Kat

(with copper, lead, zinc and the polymetallic cocktail) and downregulation of CO_2 inducible protein (in the presence of cadmium an the polymetallic cocktail). Energy metabolism was also impacted under stresses by: copper (8 % of proteins involved showed modified expression with a contrasting effect of this metal on FNR), zinc (9 % of proteins with modified expression: FNR and AdK were downregulated) and polymetallic cocktail (7 % proteins of interest: FNR being downregulated). Chaperone activity was the third most affected function, under lead (6 % with contrasting effects of this metal on HSP 60) and cadmium stress (5 % with downregulated HSP 60). The other impacted functions were: neoglucogenesis and glycolysis (between 2 % and 6 % of modified proteins) affected by copper, zinc, cadmium and the polymetallic cocktail (downregulated GAPDH, except upregulation by copper, and/or upregulation of PEP synthase in presence of copper), photorespiration by lead, zinc, cadmium and the polymetallic cocktail (systematically downregulated RUBISCO), and protein degradation by copper and the polymetallic cocktail (systematically downregulated SCP).

1.2. Effects of metals on the soluble proteome of *A. pacificum* TAR C5-4F

LC-MS/MS identification and functional annotations for the proteins modified in expression (= proteins of interest) in the TAR C5-4F strain are shown in **Table 2**.

1.2.1. Effects of copper contamination

TAR C5-4F cells exposed to copper showed 197 ± 82 spots (**Figure 5A**). This was not significantly different (Student's *t*-test: $P > 0.10$) from controls (294 ± 50 spots).

32 % of the soluble proteome varied in expression in response to copper, with 29 % proteins significantly downregulated or disappeared, and 3 % proteins significantly appeared (**Figure 5B)**. Among appeared proteins, was PP (spot 25), and downregulated or disappeared proteins were a translation initiation inhibitor (spot 17), ADSS (spot 18), proteasome subunit (spot 23), FNR (spots 43, 44, 45 and 50) and RUBISCO (spot 46). Contrasting effects of copper (appearance and downregulation for different spots of the same protein) were recorded for PCP (spots 12, 77 and 159) and HSP 70 (spots 22 and 163).

The main functions affected (**Figure 6**) were: photosynthesis (22 % of proteins of interest) with contrasting expression of PCP but disappeared/downregulated RUBISCO and FNR, then, energy metabolism (12 % of proteins of interest) with downregulated ADSS and disappeared FNR. Other functions were: the oxidative stress response (8 %, contrasting expression of HSP 70 and downregulated proteasome), protein modification, chaperone

activity and translation inhibition (4 %, upregulated PP, contrasting expression of HSP 70, and downregulated translation initiation inhibitor, respectively), and finally, photorespiration (2 %, disappeared RUBISCO).

1.2.2. Effects of lead contamination

In response to lead stress, PEP showed 201 ± 50 spots, which was nearly significantly lower (Student's *t*-test: $0.05 < P^* \leq 0.10$) of 32 % than controls (**Figure 5A**).

24 % proteins were differently expressed under this contamination: 20 % proteins were downregulated or disappeared, and 4 % proteins were upregulated or appeared (**Figure 5B**). Among appeared proteins, we found HSP 70 (spot 163) and the downregulated or disappeared proteins: translation initiation inhibitor (spot 17), ADSS (spot 18), AGMAT (spot 61), ATP synthase (spot 65), CALR (spot 68), LBP (spot 70) and MAT (spot 78). Contrasting effects of lead were observed for PCP (downregulation for spot 12, but upregulation or appearance for spots 67, 77, and 159) and PP (appearance for spot 25, but downregulation for spot 64).

Proteins of interest were assigned to photosynthesis (17 % of proteins of interest) with contrasting expression of PCP and downregulation of ATP synthase (**Figure 6**). The following functions were also impacted: energy metabolism and protein modification (8 %, downregulated ATP synthase, ADSS and contrasting effects on PP, respectively), then: chaperone activity (6 %, appeared HSP 70 and downregulated CALR), translation inhibition, metabolite biosynthesis, urea metabolism and bioluminescence (4 % for each function, downregulated translation initiation inhibitor, MAT and AGMAT, and disappeared LBP, respectively), and finally, the oxidative stress response (2 %, appeared HSP 70).

1.2.3. Effects of zinc contamination

In response to zinc stress, the PEP showed 321 ± 126 spots (**Figure 5A**). This was not significantly different (Student's *t*-test: $P > 0.10$) from controls.

10 % of the soluble proteome showed modified expression in response to zinc, among which 9 % proteins were downregulated or disappeared, and 1 % protein were appeared (**Figure 5B**). Downregulated or disappeared proteins were: HSP 70 (spot 22), FNR (spot 80), RUBISCO (spot 90), AGMAT (spot 61), PP (spot 64) and ATP synthase (spot 65). Zinc had contrasting effects on PCP (downregulation in spots 81, 82, 83, 84, but spot 159 appeared).

Photosynthesis was the first impacted (32 % of proteins of interest) with contrasting effects on PCP, disappeared RUBISCO, downregulated ATP synthase and FNR (**Figure 6**). Then, it was: energy metabolism (7 %, downregulated ATP synthase and FNR), urea metabolism (5 %, downregulation of AGMAT) and protein modification (5 %, downregulated PP). The least affected functions were: photorespiration, chaperone activity and the oxidative stress response (2 %, disappeared RUBISCO and downregulated HSP 70, respectively).

1.2.4. Effects of cadmium contamination

Under cadmium stress, the PEP showed 316 ± 75 spots, which was not significantly different (Student's *t*-test: P > 0.10) from controls (**Figure 5A**).

29 % proteins showed modified expression in response to cadmium: 25 % proteins were downregulated or disappeared, and 4 % were upregulated (**Figure 5B**). The only upregulated protein was AdK (spot 97). The following proteins were downregulated or disappeared: PCP (spots 12, 82, 83, 84, 100, 101, 102, 103, 105, 106, 107, 109 and 110), FNR (spot 80), ADSS (spot 18), proteasome subunit (spots 104 and 108), HSP 70 (spot 22), ATP synthase (spot 65), AGMAT (spot 61), PP (spot 64), CALR (spot 68), LBP (spot 76), MAT (spot 78), LAP (spot 95) and protein kinase C (spot 99).

Cadmium induced proteins mainly involved in photosynthesis (35 % of proteins of interest) with downregulated PCP, FNR and ATP synthase (**Figure 6**). Energy metabolism (8 % of proteins of interest) was also a modified pathway, with upregulated AdK, downregulated ATP synthase and FNR. Other functions were: the oxidative stress response (7 %, downregulated HSP 70 and proteasome subunit), chaperone activity (3 %, downregulated HSP 70 and CALR), energy metabolism (3 %, downregulated FNR and ATP synthase), then, it was: protein degradation and modification, bioluminescence, urea metabolism, metabolite biosynthesis and signal transduction (2 %, downregulated LAP, disappeared LBP, downregulation of AGMAT, MAT and PKC, respectively).

1.2.5. Effects of cocktail

Under polymetallic cocktail stress, the PEP showed 204 ± 61 spots (**Figure 5A**). This was nearly significantly different (Student's *t*-test: 0.05 < P* ≤ 0.10) by 30 % from the controls.

44 % proteins of interest were found: 41 % proteins were downregulated or disappeared, and 3 % proteins were appeared (**Figure 5B**). The downregulated or disappeared proteins included proteasome (spots 23, 104 and 131), FNR (spots 43, 44, 45 and 50), RUBISCO (spots 46 and 132), AGMAT (spot 61), PP (spot 64) and CALR (spot 68). The polymetallic cocktail had

contrasting effects on PCP (spots 77, 82, 83, 100, 110, 133 and 159) and HSP 70 (spots 22 and 163).

Proteins of interest were primarily assigned to (**Figure 6**): photosynthesis (29 % of proteins of interest) with contrasting effects on PCP and disappeared/downregulated RUBISCO and FNR, followed by the oxidative stress response (11 % of proteins of interest) with contrasting effects on HSP 70 and downregulation of proteasome subunit. Energy metabolism and chaperone activity (6 %, downregulated FNR, contrasting effects on HSP 70, and downregulated CALR, respectively), protein modification, urea metabolism and photorespiration (3 %, downregulated PP and AGMAT, disappeared RUBISCO, respectively) were also impacted by metals.

1.2.6. Comparison of the proteomic modifications under the different metal stresses

Lead and the polymetallic cocktail had significantly reduced the total number of proteins (by 32 % and 30 %, respectively) in the soluble proteome, whereas the other metals had no effect (Student's *t*-test: $P > 0.10$). Polymetallic cocktail led to the highest quantitative proteomic modifications (44 %), whereas zinc had the lowest impact (10 % proteins with modified expression). The polymetallic cocktail induced the highest proportion of downregulated/disappeared proteins (41 %), compared with the other metals, followed by copper (29 %), cadmium (25 %), lead (20 %) and zinc (9 %). Metals induced similar proportions of upregulated/appeared proteins, ranging from 1 % in response to zinc to 4 % in response to cadmium.

Photosynthesis was the most affected by metals with contrasting effects on PCP expression: upregulation associated with the disappearance/downregulation of FNR/RUBISCO (except with lead and/or cadmium) and downregulation of ATP synthase (with lead, zinc and cadmium). Photosynthesis was the most affected function by cadmium (35 % of proteins involved) and the least affected in by lead (17 % proteins). Except with the polymetallic cocktail (for which the second most affected function was the oxidative stress response), the second main function affected was energy metabolism, with between 6 % (polymetallic cocktail) and 12 % (copper) of proteins, through the downregulation of FNR, of ADSS (with copper and lead), and/or ATP synthase (with lead, zinc and cadmium), and occasional upregulation of AdK (with cadmium only). Another function impacted by copper, zinc, cadmium and polymetallic cocktail was the oxidative stress response (particularly with the polymetallic cocktail, which induced 11 % modifications), through downregulated proteasome (copper, cadmium and polymetallic cocktail) and downregulated and/or appeared

HSP 70. The least affected functions (between 2 % and 8 % of protein modifications) included protein modification *via* PP (upregulated with copper, contrasting effects with lead, downregulated with the polymetallic cocktail or zinc) or *via* LAP (downregulated with cadmium), chaperone activity *via* HSP 70 (appeared with lead, contrasting effects with copper or the polymetallic cocktail, downregulated with zinc or cadmium) or *via* CALR (downregulated with cadmium, lead or the polymetallic cocktail), translation inhibition (with copper or lead), photorespiration *via* RUBISCO (disappeared with copper, zinc or the polymetallic cocktail), metabolite biosynthesis *via* MAT (downregulated with lead or cadmium), bioluminescence *via* LBP (disappeared with lead or cadmium), urea metabolism *via* AGMAT (downregulated with all the metals except copper) and signal transduction *via* PKC (downregulated with cadmium).

1.3. Comparison of the proteomic modifications induced by metal stresses in both *A. pacificum* strains

Regardless of the *A. pacificum* strain, lead significantly and similarly decreased the total numbers of proteins composing the soluble proteomes. For SG C10-3, lead induced the highest proportion of downregulated/disappeared proteins. In TAR C5-4F, the polymetallic cocktail significantly reduced the total number of spots and induced the highest proportion of downregulated/disappeared proteins. In both strains, copper, zinc and cadmium had no significant effect on the total number of spots, and the stress-induced proteomic modifications mainly consisted of protein downregulation/disappearance, whatever the metals. In response to copper, cadmium and polymetallic contaminations, proportions of downregulated/disappeared proteins were higher in TAR C5-4F than in SG C10-3, whereas in presence of lead or zinc, they were higher in SG C10-3. Under cadmium stress, some proteins were downregulated in both strains: ATP synthase involved in photosynthesis and energy metabolism, PCP involved in photosynthesis, and proteasome subunit involved in the oxidative stress response (**Figure 7**). In response to copper or polymetallic stress, spots corresponding to FNR, involved in photosynthesis and energy metabolism, disappeared from both the SG C10-3 and the TAR C5-4F proteomes (**Figure 7**). Proportions of upregulated/appeared proteins were always higher in the SG C10-3 proteome than in that of TAR C5-4F. However, these proportions remained low (< 10 %) in the proteomes expressed by both strains. No upregulated protein was observed in both the SG C10-3 and the TAR C5-4F proteomes, although spots corresponding to PCP appeared in both, in response to copper, lead, zinc, and polymetallic stresses (**Figure 7**).

For both strains, photosynthesis was the main function affected by the metals, through modifications in expression of PCP (most often upregulated/appeared for SG C10-3 *vs* contrasting expression patterns for TAR C5-4F), and downregulation of FNR, RUBISCO and ATP synthase. Other functions affected differed according to the strains: the second function was the oxidative stress response for SG C10-3 (with frequent upregulation of HSP 60/apparition of proteasome with copper and polymetallic contamination, some appeared SOD with lead and zinc) *vs* energy metabolism for TAR C5-4F (occasional upregulation of AdK with cadmium), and the third was the oxidative stress response for TAR C5-4F (sometimes appeared HSP 70 with lead, copper and the polymetallic cocktail) *vs* the energy metabolism for SG C10-3 (rare upregulation of FNR with copper). Among the less affected functions, some were the same for both strains (chaperone activity and photorespiration), whereas others were affected in SG C10-3 or TAR C5-4F only (neoglucogenesis, glycolysis and protein degradation in SG C10-3, protein modification, translation inhibition, metabolite biosynthesis, bioluminescence, urea metabolism and signal transduction in TAR C5-4F).

2. Effects of metals on the PST contents in A. pacificum *cells*

2.1. In SG C10-3 strain

Among the PSTs (GTX4, GTX1, GTX5, GTX 3, GTX 2, neo-STX, C1 and C2 toxins), C2 predominated in the SG C10-3 cells, reaching an average of 42 ± 6 % of the total PSTs (max = 50 ± 3 % in response to polymetallic contamination) (**Figure 8**). GTX4 was also abundant, representing an average of 30 ± 5 % of the total PSTs (max = 39 ± 3 % in response to cadmium). GTX5 was also represented in SG C10-3 cells, with an average of 19 ± 8 % (max = 27 ± 6 % in response to cadmium). The least abundant PSTs were (% in average): GTX1 (4 %) > C1 (3 %) > GTX3 (1.4 %) > neo-STX (1.1 %) > GTX2 (0.2 %).

Total PST contents ranged from 23 ± 8 µM in controls to 57 ± 16 µM in polymetallic cocktail conditions (**Figure 9**). The polymetallic cocktail induced the highest significant level of total PSTs than did the controls (2.5 times higher) ($0.01 < P^{**} \leq 0.05$), cadmium (2.4 times higher) ($0.01 < P^{**} \leq 0.05$) and zinc (1.8 times higher) ($0.01 < P^{**} \leq 0.05$). Copper induced higher (1.8 times higher) significant total PST contents in comparison with controls ($0.01 < P^{**} \leq 0.05$), cadmium (1.8 times higher) and zinc (1.3 times higher) ($P^{***} \leq 0.01$). Other metal stresses (by lead, zinc, and cadmium) did not induce significant differences in the total PST contents.

C2 contents ranged from 4.8 ± 2.8 µM with cadmium to 28.7 ± 6.0 µM in polymetallic conditions (**Figure 9**). The polymetallic cocktail induced the highest significant level of C2 in the cells than did the controls (2.5 times higher) ($0.01 < P^{**} \leq 0.05$), cadmium (6.0 times

higher) ($P^{***} \leq 0.01$), zinc (1.9 times higher) ($0.01 < P^{**} \leq 0.05$) and copper (1.7 times higher) ($0.01 < P^{**} \leq 0.05$).

GTX4 contents varied between 6.8 ± 2.5 µM for controls and 18.5 ± 5.6 µM in cocktail conditions (**Figure 9**). As for total PSTs and C2, the polymetallic cocktail induced the highest significant level of GTX4 than did the controls (2.7 times higher) and zinc (2.1 times higher) ($0.01 < P^{**} \leq 0.05$).

GTX5 contents varied between 4.0 ± 0.5 µM with the polymetallic cocktail and 10.3 ± 2.1 µM with copper (**Figure 9**). Copper induced the highest significant level of GTX5 than did the controls (2.5 times higher) ($0.01 < P^{**} \leq 0.05$) and it also induced the highest significant levels of GTX1 and C1 in the cells ($0.01 < P^{**} \leq 0.05$).

Under different metal stresses, there were some significant positive correlations (Spearman's test: $P \leq 0.05$) between the PSTs: C2 and total PSTs (r = 0.94), GTX4 and total PSTs (r = 0.83)/GTX1(r = 0.89)/C1 (r = 0.89), GTX1 and GTX2 (r = 0.83), C1 and GTX2 toxins (r = 0.83).

Significant positive correlations (Spearman's test: $P \leq 0.05$) were found under different metal stresses, between total PSTs and PCP (involved in photosynthesis) (spots 170 and 210) (r = 0.83 and 0.89, respectively), C2 toxins and PCP (spots 68 and 170) (r = 0.83 for both spots), GTX4 and PCP (spot 210) (r = 0.89), GTX1 and PCP (spot 210) (r = 0.83), C1 and PCP (spot 210) (r = 0.83). There were some significant negative correlations (Spearman's test: $P \leq 0.05$) between total PSTs and SOD (involved in oxidative stress response) (spot 48) (r = -1.00)/FNR (spot 114) (r = -0.83)/SCP (spot 16) (r = -0.83), C2 and SOD (spot 48) (r = -0.94), GTX4 and SCP (spot 194) (r = -0.83)/FNR (spot 40) (r = -0.94)/SOD (spot 48) (r = -0.83), GTX5 and PCP (spot 205) (r = -0.83), neo-STX and RUBISCO (spot 119) (r = -0.94).

2.2. In TAR C5-4F strain

Among the different PSTs, GTX4 was predominant regardless the conditions, reaching an average of 48 ± 6 % of the total PSTs (max = 52 ± 8 % with cadmium) (**Figure 8**). C2 was also abundant, representing an average of 37 ± 4 % of the total PSTs (max = 41 ± 3 % with lead). GTX5 was also represented in the TAR C5-4F cells, with an average of 7 ± 4 % of the total PSTs (max = 11 ± 5 % with copper). The least abundant PSTs in the cells were (% in average): GTX1 (5 %) > C1 (2 %) > neo-STX (1 %) > GTX3 (0.08 %) > GTX2 (0.02 %).

Total PSTs ranged from 17 ± 7 µM in response to cadmium to 28 ± 9 µM in response to lead (**Figure 9**). In comparison with controls, none of the metal conditions induced significant differences in the total PSTs produced by TAR C5-4F (Student's *t*-test: $P > 0.10$).

Metals did not induce significant differences in GTX4 in comparison with controls (from 8.9 ± 3.0 µM with cadmium, to 14.1 ± 4.3 µM in controls) (Student's *t*-test: P > 0.10) (**Figure 9**). Metals had no effect on C2 compared with controls (from 6.1 ± 3.1 µM with cadmium, to 11.4 ± 4.1 µM with copper) (**Figure 9**). Regarding GTX5, in comparison with controls, copper induced significantly different contents (2.2 times higher) in the cells ($0.01 < P^{**} \leq 0.05$) (**Figure 9**).

Under metal stresses, some significant positive correlations (Spearman's test: $P \leq 0.05$) were observed between the PSTs: GTX4 and total PSTs (r = 0.94)/C2 (r = 0.89)/neo-STX (r = 0.94), C2 and total PSTs (r = 0.94), GTX5 and GTX2 (r = 0.82), GTX1 and total PSTs (r = 0.83), C1 and GTX2 (r = 0.94), neo-STX and total PSTs (r = 0.83).

Significant positive correlations (Spearman's test: $P \leq 0.05$) were found under different metal stresses, between total PSTs and PCP (spots 83, 100, 102, and 107) (r = 0.94, 1.00, 0.83, and 0.83, respectively), C2 and PCP (spots 82, 83, 100, 102, and 106) (r = 0.89, 0.89, 0.94, 0.89, and 0.83, respectively), C2 and HSP 70 (spot 22) (r = 1.00), GTX4 and PCP (spots 83 and 102) (r = 0.83 and 0.94, respectively), GTX4 and HSP 70 (spot 22) (r = 0.89)/LBP (spot 76) (r = 0.94), GTX1 and PCP (spot 100) (r = 0.83), neo-STX and LAP (spot 95) (r = 0.83)/LBP (spot 76) (r = 0.88)/PCP (spot 100) (r = 0.83). There were significant negative correlations (Spearman's test: $P \leq 0.05$) between GTX5 and AdK (spot 97) (r = -0.89), C1 toxins and AdK (spot 97) (r = -0.94), GTX3 and PCP (spots 101 and 103) (r = -0.83 for both spots), GTX2 and AdK (spot 97) (r = -0.94)/proteasome subunit (spot 23) (r = -0.82).

Discussion

1. Proteomic responses to metal stresses

According to Zhan et al. (2021), 2-DE is a well-established technical platform enabling extensive proteomic analysis that has impacted its application to in-depth investigations of proteomes at the level of protein species/proteoforms. Each detectable spot contains multiple proteoforms derived from the same gene, as well as from different genes. Proteoforms derived from the same gene are distributed into different spots in a 2-DE pattern. Thanks to 2-DE, each proteoform can be resolved and arrayed according to its isolelectric points and molecular weights. 2-DE coupled with LC-MS/MS has tremendous potential for the large-scale detection, identification and quantification of the proteoforms that constitute proteomes. Here, regardless of the metal stress and the *A. pacificum* strain tested, the proteomic responses mainly consisted of downregulation or disappearance of proteins constituting the soluble proteomes. Metals generate oxidative stress producing reactive oxygen species (ROS), which

oxidize polypeptide sequences of proteins, then, damaged proteins are targeted by ubiquitination for subsequent proteasomal degradation (Flick and Kaiser, 2012). This could contribute to explain the lower protein abundances here observed in the soluble proteomes of the *A. pacificum* strains exposed to metal stresses. However, in response to environmental changes, organisms can also modify themselves their proteomes. The involved proteomic modifications are intended to activate or slow down the metabolic pathways based on the differentially expressed proteins, to face to the environmental changes experienced: they are at the basis of the adaptive organism responses to stresses (Jean at al., 2017).

Lead stress significantly decreased the total number of proteins composing the proteomes of both strains. In strain SG C10-3, lead was the metal that induced the strongest impact, with the highest proportions of downregulated/disappeared proteins. Similarly, the proteome of the red macroalga *Gracilaria lemaneiformis* exposed to lead revealed 14 proteins significantly differentially expressed and identified, among which 11 were downregulated (Du et al., 2018). In strain TAR C5-4F, polymetallic stress (cocktail) also significantly reduced the total number of proteins, inducing the highest proportions of downregulated/disappeared proteins. Lead or zinc affected the proportions of downregulated/disappeared proteins in strain SG C10-3 more than in strain TAR C5-4F, but copper, cadmium, or the polymetallic cocktail had more effects on strain TAR C5-4F than on strain SG C10-3. For all the metals tested, proportions of upregulated/appeared proteins (< 10 % of the proteins with modified expression in both strains) were higher in SG C10-3 than in TAR C5-4F. These results showed differences in the proteomic responses of the two *A. pacificum* strains exposed to metal stresses. Similarly, proteomic differences in response to cadmium stress have been observed in two strains of the green microalga *Euglena gracilis* (the *Z*-strain and the sugar-loving *E. gracilis* var. *saccharophila* B-strain): 960 proteins in the *Z*-strain and 127 proteins in the B-strain changed in relative abundance compared with the untreated control, with upregulated proteins including the major facilitator superfamily (MFS) transporters, cadmium/zinc-transporting ATPase, heavy metal transporting P1B-ATPase and thiol-rich proteins involved in metal chelation/sequestration/cellular stress response (Khatiwada et al., 2020). Similary, in two strains of the brown alga *Ectocarpus siliculosus*, the Es32 strain was more sensitive to copper stress than the Es524 strain, with (*i*) toxicity detected at levels as low as 50 μg L^{-1} Cu, whereas Es524 displayed negative effects only from exposure to 250 μg L^{-1} Cu, and (*ii*) differential soluble proteome profiling for each strain, showing, in Es524, striking expression of PSII Mn- stabilizing protein, fucoxanthin chlorophyll *a–c* binding protein, RNA helicases and vanadium- dependent bromoperoxidase (Ritter et al., 2010). Here, the

proteomic responses obtained are also based on two *A. pacificum* strains only, and may differ when experimenting with other strains due to potential intraspecific variability.

1.1. Response involved in photosynthesis

In both strains, the impacts of metals on the *A. pacificum* proteomes were mainly observed as modifications in the expression of proteins involved in photosynthesis. Among the photosynthetic proteins modified in expression, the peridinin chlorophyll *a* binding protein (PCP) was upregulated/appeared in both strains, but more often in SG C10-3 than in TAR C5-4F, *i.e.* under copper, lead, zinc, or polymetallic (cocktail) stress. PCP is the major constituent of the light-harvesting complex that binds both chlorophyll *a* and the carotenoid peridinin, an accessory pigment found in dinoflagellates (Le et al., 1997). The proteome of *G. lemaneiformis* exposed to lead, also showed upregulated photosynthetic proteins (cytochrome b6-f complex iron-sulfur subunit) (Du et al., 2018), whereas higher expression of the photosynthetic fucoxanthin chlorophyll *a–c* binding protein has been reported for *E. siliculosus* (strain Es524) exposed to copper (Ritter et al., 2010). Our results suggest that, under metallic stress conditions, the studied *A. pacificum* strains, particularly SG C10-3, could upregulate PCP to increase their photosynthetic pathway: one advantage may be more photosynthesized organic matter in response to a greater energy demand arising from increased cellular metabolism under metal stress, and in metal-contaminated ecosystems, to ensure the cell survival in these conditions.

However, other photosynthetic proteins such as ribulose bisphosphate carboxylase (RUBISCO), chloroplast ferredoxin-NADP(+) reductase (FNR) and ATP synthase were generally downregulated/disappeared in the both *A. pacificum* proteomes, which reveals the contrasting effects of the metal stresses, some of which have adverse effects on the photosynthesis. RUBISCO catalyzes carboxylation of the substrate ribulose-1,5-bisphosphate (RuBP) during the second step of photosynthesis (Reuman and Weber, 2006), whereas the FNR enzyme is involved in the photophosphorylation step during photosynthesis (Jean et al., 2017). Here, the decrease in the expression of RUBISCO/FNR/ATP synthase indicates that photosynthesis and the mitochondrial energy mechanism may have been damaged under oxidative stress generated by metals, as explained above. Similarly, metalrich natural water has a drastic effect on the soluble proteome of *Chlamydomonas* sp., with a decrease in the abundance of RUBISCO, as well as other enzymes related to photosynthesis (Cid et al., 2010). Another study mentions that the exposure of the green microalga *Chlorella sorokiniana* to 250 µM Cd^{2+} for 40 h causes downregulation of photosynthesis of (Leon-Vaz

et al., 2021). In the brown alga *Sargassum fusiforme*, proteins related to photosynthesis are significantly reduced in response to acute copper stress (Zou et al., 2015). Metals such as copper also affected photosynthesis-related proteins (proteins associated with light harvesting complexes) in the marine diatom *Thalassiosira oceanica* (Kong and Price, 2020). A study investigating the response of the rice leaf proteome to various metals showed that the photosynthesis apparatus was severely disrupted under metal stress, with degradation of some photosynthetic pathway-related proteins, including RUBISCO (Hajduch et al., 2001). In the present study, the comparison of the metal effects on strain SG C10-3 showed that the polymetallic cocktail induced the strongest modifications on its photosynthetic proteins, whereas the lowest impact was recorded under copper stress. Different results were obtained for strain TAR C5-4F, because its photosynthetic proteins were the most modified in expression by cadmium, and the least impacted by lead, which confirms the variability in the proteomic responses of the two strains exposed to metal stresses. The minimum inhibitory concentration (MIC) in the flagellate microalga *E. gracilis* exposed to cadmium, lead and mercury decreases in the order of Pb > Cd > Hg, which reflects our results regarding the respective effects of cadmium or lead on photosynthetic proteins expressed by *A. pacificum* TAR C5-4F (Khatiwada et al., 2020).

1.2. Response involved in oxidative stress

The response to oxidative stress was the second biological function most affected by metal stresses in SG C10-3, whereas it was the third in TAR C5-4F. In SG C10-3, metal-induced response to oxidative stress may be enhanced *via* upregulated proteins: (*i*) heat shock protein (HSP) 60 was upregulated in response to stresses by copper, lead, zinc or cadmium, (*ii*) proteasome subunit as sometimes upregulated in response to copper or polymetallic contamination, and (*iii*) superoxide dismutase (SOD) was upregulated in response to lead or zinc stresses. Evolutionarily conserved HSPs are so named because they are upregulated by organisms during an acute increase in temperature, but a variety of other stresses including extreme ion concentrations, high light levels, dehydration, cellular energy deprivation and oxidative stress can also induce them (Gerloff-Elias et al., 2006). Similarly, accumulation of HSPs was observed in *E. siliculosus* under exposure to copper (Ritter et al., 2010). SOD minimizes oxidative cell damage in organisms, particularly in polluted environments (Okamoto and Colepicolo, 1998) and participates in the first antioxidant response to the reactive oxygen species (ROS) generated by metal stress (Bareen et al., 2012). The proteasome contributes to proteolytic activity of the cells and plays a major role in the

oxidative stress response by eliminating oxidized proteins, which have been beforehand targeted by ubiquitination (Jean et al., 2017). Studies have reported a significant increase in abundance of ubiquitinated proteins in cells exposed to metals (Marzano et al., 2012). Upregulation of some antioxidation proteins has also been observed in *C. sorokiniana* cells exposed to 250 μM Cd^{2+} (Leon-Vaz et al., 2021), the marine alga *Scytosiphon gracilis* exposed to 100 μg L^{-1} Cu (Contreras et al., 2010), *G. lemaneiformis* exposed to lead, with higher contents in SOD, peroxidase and glutathione transferase (Du et al., 2018).

In TAR C5-4F, the response to oxidative stress under metal contamination may also be enhanced by upregulated HSP 70 (in response to copper, lead, or polymetallic contamination), but in contrast, proteasome subunits were always downregulated in this strain under metal stresses. In *Chlamydomonas* sp. cells grown in metal- rich water, and in *G. lemaneiformis* exposed to lead, HSP 70 is also upregulated in response to metal stresses (Cid et al., 2010; Du et al., 2018). An antioxidant strategy is based on the repair of damaged proteins by inducing the synthesis of HSPs, which function as chaperones to maintain cellular homeostasis. These proteins promote cellular redox homeostasis by stimulating antioxidant systems and preventing protein aggregation under stress conditions (Leon-Vaz et al., 2021). In the present study, upregulated HSPs, proteasome and SOD, particularly in SG C10-3, appear to suggest some defense capacities under metal stress conditions. Taking metal sustainability in coastal ecosystems in account, Siano et al. (2021) showed that metal contamination leads to plankton shifts, particularly in favor of dinoflagellates (*e.g*. *Alexandrium*) able to form dormant cysts in the sediments. Our results corroborate the survival capacity of *A. pacificum* in the presence of metals, contributing to its development in metal-contaminated ecosystems.

1.3. Response involved in energy metabolism

Energy metabolism was the second biological function most affected by metal stresses in TAR C5-4F, but was the third in the SG C10-3 strain. In SG C10-3, energy metabolism was impacted by metal contamination, as shown by downregulation of ATP synthase and adenosine kinase (AdK), under cadmium or zinc stress, respectively. Similar results were obtained for TAR C5-4F, with downregulation of (*i*) ATP synthase, in response to lead, zinc or cadmium stress and (*ii*) adenylosuccinate synthetase (ADSS), in response to copper, lead or cadmium stress. However, in this strain, AdK was upregulated in response to cadmium stress. Compared with the well-known ATP synthase, AdK is an evolutionary ribokinase widely expressed in all forms of life, catalyzing the transfer of phosphate from adenosine triphosphate (ATP) to adenosine, which leads to the formation of adenosine monophosphate

(AMP) (Boison and Jarvis, 2020). Upregulation of this protein, and downregulated ATP synthase and ADSS highlight the contrasting effects of cadmium on energy metabolism of this strain. The ADSS enzyme is important in purine biosynthesis, because it catalyzes the guanosine triphosphate (GTP)-dependent conversion of inosine monophosphate (IMP) and aspartic acid to guanosine diphosphate (GDP), phosphate and N(6)-(1,2-dicarboxyethyl)-AMP (Feng et al., 2015). In *S. fusiforme* cultivated in the presence of copper, the expression of energy metabolism-related proteins is significantly reduced in response to acute copper stress, but induced by chronic copper stress (Zou et al., 2015). Similarly, *G. lemaneiformis* exposed to lead also downregulates these proteins (Du et al., 2018). These results agree with our findings showing the general harmful effects of metals on the energy metabolism of the two studied *A. pacificum* strains.

1.4. Response involved in other metabolic functions

Other metabolic functions were also impacted by metal stresses, but to a lesser degree than the above-mentioned ones, *i.e.* with lower differences in protein expression in the respective proteomes. In the SG C10-3 strain, in response to copper glyceraldehyde-3-phosphate dehydrogenase (GAPDH) and phosphoenolpyruvate (PEP) synthase were upregulated. Similarly, in *S. gracilis*, copper also upregulates GAPDH (Contreras et al., 2010); however, in the marine microalga *Nannochloropsis oculata*, cadmium causes a loss of GAPDH from the proteome (Kim et al, 2005). GAPDH is a glycolytic enzyme known to regulate the expression of proteins by binding to mRNAs, and its increased expression is observed under oxidative stress. Indeed, this enzyme is required to maintain energy, reducing power and controlling the generation of H_2O_2 under oxidative stress conditions (Contreras et al., 2010). PEP synthase catalyzes the energetically favorable synthesis of phosphoenolpyruvate from pyruvate and ATP (Eyzaguirre et al., 1982). Thus, in the SG C10-3 strain, upregulated GAPDH may attenuate the negative effects of oxidative stress caused by copper, whereas the upregulation of PEP synthase may help provide more energy for the cell survival under exposure to this metal. In the TAR C5-4F strain, protein modification may be enhanced by the upregulation of serine/threonine-protein phosphatase (PP) observed in response to copper or lead stress. PP contributes to the control of phosphorylation in structural and regulatory proteins in eukaryotes (Wera and Hemmings, 1995). This means that PP upregulation in TAR C5-4F under metal stress conditions may improve the turnover of some proteins involved in major pathways. RUBISCO, also involved in the photorespiratory pathway, was downregulated in

both *A. pacificum* strains exposed to metals, which does not corroborate the upregulation of photorespiration observed in the *C. sorokiniana* cells exposed to cadmium (Leon-Vaz et al., 2021). Other metabolic functions may be downregulated in the *A. pacificum* strains, such as: (*i*) translation initiation inhibition in TAR C5-4F exposed to copper or lead, which may indicate that protein translation mechanism is activated in favor of TAR C5-4F survival in these conditions; (*ii*) proteolytic activity or signal transduction in TAR C5-4F exposed to cadmium (leucine aminopeptidase or protein kinase C, respectively downregulated); (*iii*) metabolite biosynthesis or bioluminescence in TAR C5-4F exposed to lead or cadmium (methionine S-adenosyl transferase or Luciferin-binding protein, downregulated), (*iv*) urea metabolism in TAR C5-4F exposed to all metal stresses (except with copper) (downregulated agmatinase) and (*v*) protein degradation in SG C10-3 exposed to copper or the polymetallic cocktail (serine carboxypeptidase was downregulated).

2. PST production in response to metal stresses

Regardless of the conditions, C2 or GTX4, followed by GTX5, were the most abundant PSTs in the two *A. pacificum* strains, whereas the least abundant toxins were, in descending order: GTX1, C1, GTX3 or neo-STX and GTX2. These results corroborate those obtained by Laabir et al. (2013) for the *A. pacificum* strain ACT03 (isolated from Thau Lagoon, French Mediterranean coast), which produced GTX3, GTX4, GTX5, C1, C2, C3 and C4, with predominance of C2 at 12-18°C and salinities 10-25 psu whereas GTX5 was dominant at 21-30°C at almost all salinities. Similarly, eight other French *A. pacificum* strains mainly produced C2, GTX4 and/or GTX5 (Geffroy et al., 2021). In a Chilean strain of *A. pacificum*, C1, C2, B1, GTX1 and GTX4 composed more than 90 % of the total PSTs, this composition being consistent with that determined for *A. pacificum* populations from the Pacific coast (Krock et al., 2007). In other Chilean strains named PFB38, PFB42 and PFB37, more than 98 % of the total PSTs occurred in the form of (in decreasing order) GTX4, GTX1, GTX3 and GTX2, whereas in the strains PFB39, PFB36 and PFB45, neo-STX and STX toxins were detected (Aguilera-Belmonte et al., 2011). Predominance of GTX6 has been recorded in most of the 30 *A. pacificum* strains coming from the Annaba Bay (Algeria) (Hadjadji et al., 2020). The toxin profile of an *A. pacificum* strain from the Bizerte Lagoon was composed of C1, GTX6 and neo-STX (which represented 2.8 % of the total PSTs) (Fertourna-Bellakhal et al., 2015). In axenic *A. pacificum* cultures exposed to different nutrient conditions, the following

order was found for toxin biosynthesis: C1 or C2 > GTX3 > GTX1 > neo-STX (Han et al., 2016), confirming, as we observed, the main contribution of C2 compared with neo-STX.

Under the various conditions, we recorded clear differences between the SG C10-3 and TAR C5-4F toxin profiles. Higher contents in SG C10-3 than in TAR C5-4F were measured in control conditions for GTX5 ($P^{***} \leq 0.01$), and in response to (*i*) polymetallic stress (cocktail) for total PSTs ($0.01 < P^{**} \leq 0.05$), C2 ($P^{***} \leq 0.01$), GTX5 ($0.01 < P^{**} \leq 0.05$) and neo-STX ($P^{***} \leq 0.01$), (*ii*) copper ($P^{***} \leq 0.01$), lead ($0.01 < P^{**} \leq 0.05$) or zinc ($P^{***} \leq 0.01$) stress for GTX5, (*iii*) copper or cadmium stress ($0.01 < P^{**} \leq 0.05$) for neo-STX and (*iv*) zinc stress for GTX3 ($P^{***} \leq 0.01$) (Figure 9). Variability in toxin production has also been found among the numerous *A. pacificum* strains from Annaba Bay (Algeria) (Hadjadji et al., 2020). Similarly, variability has also been detected among Chilean *A. pacificum* strains, with the highest contents in strain PFB45, and the lowest in strain PFB4 (Aguilera-Belmonte et al., 2011). For the two strains studied here, the various PSTs were significantly positively correlated under the metal stresses tested, showing the same patterns in PST synthesis under the different metal conditions. In SG C10-3 cells, the polymetallic cocktail, which represents the most frequent type of metal contamination in ecosystems, induced the highest total PSTs, C2 and GTX4 contents, whereas copper increased total PSTs and induced the highest GTX5, GTX1 and C1 contents compared with controls. Previous studies mention similar results, showing that increasing copper concentrations induce significant overproduction of PSTs in *A. pacificum* (Couet et al., 2018). By contrast, metals did not have significant effects on the toxin production in TAR C5-4F, except copper stress that significantly increased the GTX5 content. Increased Cu^{2+} levels stimulated STX production in the cyanobacterium *Raphidiopsis raciborskii* (Giraldi et al., 2021). It has been hypothesized that STXs could bind to metal transporters, contributing to decrease the stress triggered by metals on microorganisms. Phycotoxin production is also enhanced by metals in several microalgal species: *Pseudo-nitzschia australis* (in the presence of copper or zinc), *Karenia selliformis* (by adding selenium and magnesium), *Ostreopsis siamensis* (in presence of copper), *Prorocentrum lima* (in presence of copper) and *Prorocentrum reticulatum* (addition of selenium) (Rhodes et al., 2006). Consequently, metals and subsequent increases in algal bloom toxicity may increase the impact of HABs on neural system syndromes, mass mortalities of fish, shellfish, marine mammals and birds, and for aquaculture or shellfish farming.

For both *A. pacificum* strains exposed to the different conditions, significant positive correlations were found between, on the one hand, total PSTs, C2, GTX4, GTX1, and on the other hand, the expression of the photosynthetic PCP protein. Moreover, although toxin

production was enhanced under polymetallic and copper stresses in strain SG C10-3, apparition of photosynthetic PCP was observed in common under these contaminated conditions. Significant positive correlations were also observed (*i*) between C1 and PCP in SG C10-3 and (*ii*) between neo-STX and PCP in TAR C5-4F. These results suggest that toxin biosynthesis and photosynthesis (represented by PCP) may be linked in *A. pacificum*, and this putative relationship should be directly tested in future investigations. For instance, comparison of the protein profiles of toxic and non-toxic *A. pacificum* strains has shown that photosynthetic proteins are upregulated in the toxic strain, suggesting that these proteins are also involved in toxin biosynthesis (Tse et al., 2020), providing further support for our hypothesis. Similarly, 210 proteins exhibiting differential expression in *A. pacificum* cells, during four stages of the toxin biosynthesis, including upregulated proteins involved in photosynthesis, also indicate relationships between these two processes (Zhang et al., 2018). A study comparing the protein profiles between a toxicity-less mutant and a wild toxic *A. pacificum* showed differentially expressed proteins involved in the photosynthesis of the mutant, which suggests that these proteins may be involved in the toxin biosynthesis (Wang et al., 2012). Proteins involved in photosynthesis (phosphoenolpyruvate carboxylase, chloroplast phosphoglycerate kinase, Mg^{2+} transporter protein and chloroplast phosphoglycerate kinase) have shown increased expression during PST synthesis in *Alexandrium tamarense* CI01 (Jiang et al., 2015). Consequently, some photosynthetic proteins could be involved in the *Alexandrium* toxin biosynthesis, without excluding that, PSTs being secondary metabolites, PST correlation with photosynthesis also could be the result of metabolic activity and growth (photosynthesis) of cells producing toxins.

Other significant positive correlations were found, but only in TAR C5-4F, between (*i*) on the one hand, C2 and GTX4, and on the other hand, expression of HSP 70 (involved in chaperone activity), (*ii*) GTX4/neo-STX and expression of LBP (involved in bioluminescence) and (*iii*) neo-STX and expression of LAP (involved in proteolytic activity). Therefore, these correlations may also point to a link between toxin biosynthesis and chaperone activity, bioluminescence and/or proteolytic activity.

Conversely, negative significant correlations were found in SG C10-3 between (*i*) on the one hand, total PSTs, C2, GTX4, and on the other hand, expression of SOD (involved in the response to oxidative stress), (*ii*) total PSTs, GTX4 and expression of FNR (involved in energy metabolism) and SCP (involved in protein degradation). In TAR C5-4F, there were negative correlations between GTX5/C1/GTX2 and expression of AdK (involved in energy metabolism), and between GTX2 and expression of proteasome (involved in the response to

oxidative stress). Another study mentions that energy production-related proteins were upregulated in a toxic strain of *A. pacificum*, compared with the protein profile of a non-toxic strain, suggesting that these proteins are also involved in toxin biosynthesis (Tse et al., 2020). Comparison of the protein profiles of *A. pacificum* at different toxin biosynthesis stages has demonstrated differentially expressed proteins involved in response to oxidative stress (Wang et al., 2013). In the present study, the negative correlations observed suggest that energy metabolism and response to oxidative stress may be more effective pathways than toxin biosynthesis - perhaps even to its detriment - in the two studied *A. pacificum* strains when they are exposed to metal stresses.

Conclusions

The harmful effects of metals on the soluble proteomes expressed by two *A. pacificum* strains could be countered by the upregulation of some proteins involved in photosynthesis (PCP), oxidative stress response (HSP 60/70, proteasome and SOD), energy metabolism (AdK), neoglucogenesis and glycolysis (GAPDH and PEP synthase) and protein modification (PP). These proteins may contribute to the adaptive proteomic responses of the two *A. pacificum* strains, enhancing their survival in metal contaminated ecosystems. However, under the metal stresses tested, these two strains showed different modifications of their soluble proteomes and different toxin profiles: SG C10-3 upregulated more proteins in its proteome; polymetallic stress had significant effects on the PST production in SG C10-3 (inducing the highest total PSTs, C2 and GTX4 contents) and induced significantly higher contents in total PSTs, C2, GTX5 and neo-STX in SG C10-3 than in TAR C5-4. For both strains, there were significant correlations between PSTs and photosynthetic PCP, may be relating photosynthesis to PST production in the *A. pacificum* cells.

Acknowledgments

This work was supported by the GdR research network "PHYCOTOX: Des micro-algues aux risques pour l'Homme et l'écosystème". We would like to thank D[rs] Antonella Luglié and Esther Garcés for their contribution to obtaining the Mediterranean *A. pacificum* strains used in this study, and D[rs] Yong Zhang and Da-Zhi Wang (State Key Laboratory of Marine Environmental Science/College of the Environment and Ecology, Xiamen University, Xiamen, P.R. China) for the *A. pacificum* protein database sequences used for protein identification.

References

Aguilera-Belmonte, A., Inostroza, I., Franco, J.M., Riobo, P., Gomez, P.I., 2011. The growth, toxicity and genetic characterization of seven strains of *Alexandrium catenella* (Whedon and Kofoid) Balech 1985 (Dinophyceae) isolated during the 2009 summer outbreak in southern Chile. Harmful Algae 12, 105-112.

Aloui, A., Recorbet, G., Lemaître-Guiller, C., Mounier, A., Balliau, T., Zivy, M., Wipf, D., Dumas-Gaudot, E., 2018. The plasma membrane proteome of *Medicago truncatula* roots as modified by arbuscular mycorrhizal symbiosis. Mycorrhiza 1, 1-16.

Anderson, D.M., Alpermann, T.J., Cembella, A.D., Collos, Y., Masseret, E., Montresor, M., 2012. The globally distributed genus *Alexandrium*: multifaceted roles in marine ecosystems and impacts on human health. Harmful Algae 14, 10-35.

Bae, M.S., Cho, E.J., Choi, E.Y., Park, O.K., 2003. Analysis of the *Arabidopsis* nuclear proteome and its response to cold stress. Plant J. 36, 652-663.

Bareen, F., Shafiq, M., Jamil, S., 2012. Role of plant growth regulators and a saprobic fungus in enhancement of metal phytoextraction potential and stress alleviation in pearl millet. J. Hazard. Mater. 237-238, 186-193.

Boison, D., Jarvis, M.F., 2020. Adenosine kinase: a key regulator of purinergic physiology. Biochem. Pharmacol., 114321.

Bravo, I., Vila, M., Masó, M., Figueroa, R.I., Ramilo, I., 2008. *Alexandrium catenella* and *Alexandrium minutum* blooms in the Mediterranean Sea: Toward the identification of ecological niches. Harmful Algae 7, 515-522.

Caruana, A.M.N., Le Gac, M., Hervé, F., Rovillon, G.-A., Geffroy, S., Malo, F., Abadie, E., Amzil, Z., 2020. *Alexandrium pacificum* and *Alexandrium minutum*: Harmful or environmentally friendly? Mar. Environ. Res. 160, 105014.

Chetouhi, C., Laabir, M., Masseret, E., Jean, N., 2019. *In silico* prediction of the secretome from the invasive neurotoxic marine dinoflagellate *Alexandrium catenella*. Environ. Microbiol. Rep. 11(4), 571-580.

Chetouhi, C., Masseret, E., Satta, C.T., Balliau, T., Laabir, M., Jean, N., 2020. Intraspecific variability in membrane proteome, cell growth, and morphometry of the invasive marine neurotoxic dinoflagellate *Alexandrium pacificum* grown in metal-contaminated conditions. Sci. Tot. Environ. 715, 136834.

Cid, C., Garcia-Descalzo, L., Casado-Lafuente, V., Amils, R., Aguilera, A., 2010. Proteomic analysis of the response of an acidophilic strain of *Chlamydomonas* sp. (Chlorophyta) to natural metal-rich water. Proteomics 10, 2026-2036.

Contreras, L., Moenne, A., Gaillard, F., Potin, P., Corre, J.A., 2010. Proteomic analysis and identification of copper stress-regulated proteins in the marine alga *Scytosiphon gracilis* (Phaeophyceae). Aquat. Toxicol. 96, 85-89.

Couet, D., Pringault, O., Bancon-Montigny, C., Briant, N., Elbaz-Poulichet, F., Delpoux, S., Kéfi-Daly, O., 2018. Effects of copper and butyltin compounds on the growth, photosynthetic activity and toxin production of two HAB dinoflagellates: The planktonic *Alexandrium catenella* and the benthic *Ostreopsis* cf. *ovata*. Aquat. Toxicol. 196, 154-167.

Craig, R., Beavis, R.C., 2004. TANDEM: matching proteins with Tandem mass spectra. Bioinformatics 20, 1466-1467.

Du, H., Lian, H., Jiang, Y., Qu, X., Yan, H., Liu, X., 2018. Proteome respeonses of *Gracilaria lemaneiformis* exposed to lead stress. Mar. Pollut. Bull. 135, 311-317.

Eyzaguirre, J., Jansen, K., Fuchs, G., 1982. Phosphoenolpyruvate synthetase in *Methanobacterium thermoautotrophicum*. Arch. Microbiol. 132, 67-74.

Feng, T., Yang, Z., Zheng, J., Xie, Y., Li, D., Murugan, S., Yang, W., Liu, J., Li, H., 2015. Examination of metabolic responses to phosphorus limitation via proteomic analyses in the marine diatom *Phaeodactylum tricornutum*. Sci. Rep. 5, 1037.

Fertouna-Bellakhal, M., Dhib, A., Fathalli, A., Bellakhal, M., Chomérat, N., Masseret, E., Laabir, M., Turki, S., Aleya, L., 2015. *Alexandrium pacificum* Litaker sp. nov (Group IV): Resting cyst distribution and toxin profile of vegetative cells in Bizerte Lagoon (Tunisia, Southern Mediterranean Sea). Harmful Algae 48, 69-82.

Flick, K., Kaiser, P., 2012. Protein degradation and the stress response. Semin. Cell Dev. Biol. 23(5), 515-522.

Garnier, C., Mounier, S., Benaïm, J.-Y., 2004. Metal logarithmic scale titration as a tool for complexing ligand distribution determination: an application by DPASV. Environ. Technol. 25, 589-599.

Geffroy, S., Lechat, M.M., Le Gac, M., Rovillon, G.A., Marie, D., Bigeard, E., Malo, F., Amzil, Z., Guillou, L., Caruana, A.M.N., 2021. From the sxtA4 gene to saxitoxin production: what controls the variability among *Alexandrium minutum* and *Alexandrium pacificum* strains? Front. Microbiol. 12, 613199, https://doi.org/10.3389/fmicb.2021.613199.

Gerloff-Elias, A., Barua, D., Molich, A., Spijkerman, E., 2006. Temperature- and pH-dependent accumulation of heat-shock proteins in the acidophilic green alga *Chlamydomonas acidophila*. FEMS Microbiol. Ecol. 56, 345-354.

Giraldi, L.A., Vargas, S.R., Santos, P.V., Tonietto, A.E., Winck, F.V., Calijuri, M. do C., 2021. Growth and saxitoxin production responses to copper ($CuCl_2$) exposure by the cyanobacterium *Raphidiopsis raciborskii*. J. Appl. Phycol. 33, 891-900.

Guillard, R.R., Ryther, J.H., 1962. Studies of marine planktonic diatoms. I. *Cyclotella nana* Hustedt, and *Detonula confervacea* (cleve). Gran. Can. J. Microbiol. 8, 229-239.

Hadjadji, I., Laabir, M., Frihi, H., Collos, Y., Shao, Z.J., Berrebi, P., Abadie, E., Amzil, Z., Chomérat, N., Rolland, J.-L., Rieuvilleneuve, F., Masseret, E., 2020. Unsuspected intraspecific variability in the toxin production, growth and morphology of the dinoflagellate *Alexandrium pacificum* R.W. Litaker (Group IV) blooming in a South Western Mediterranean marine ecosystem, Annaba Bay (Algeria). Toxicon 180, 79-88.

Hajduch, M., Rakwal, R., Agrawal, G.K., Yonekura, M., Pretova, A., 2001. High-resolution two-dimensional electrophoresis separation of proteins from metal-stressed rice (*Oryza sativa* L.) leaves: drastic reductions/fragmentation of ribulose-1,5-bisphosphate carboxylase/oxygenase and induction of stress-related proteins. Electrophoresis 22, 2824-2831.

Hallegraeff, G.M., 1993. A review of harmful algal blooms and their apparent global increase. Phycologia 32, 79-99.

Han, M., Lee, H., Anderson, D.M., Kim, B., 2016. Paralytic shellfish toxin production by the dinoflagellate *Alexandrium pacificum* (Chinhae Bay, Korea) in axenic, nutrient-limited chemostat cultures and nutrient-enriched batch cultures. Mar. Pollut. Bull. 104, 34-43.

Herzi, F., Jean, N., Sakka Hlaili, A., Mounier, S., 2014. Three-dimensional (3-D) fluorescence spectroscopy analysis of the fluorescent dissolved organic matter released by the marine toxic dinoflagellate *Alexandrium catenella* exposed to metal stress by zinc or lead. J. Phycol. 50, 665-674.

Herzi, F., Jean, N., Zhao, H., Mounier, S., Mabrouk, H.H., Hlaili, A.S., 2013. Copper and cadmium effects on growth and extracellular exudation of the marine toxic dinoflagellate *Alexandrium catenella*: 3D-fluorescence spectroscopy approach. Chemosphere 93, 1230-1239.

Hoagland, P., Anderson, D.M., Kaoru, Y., White, A.W., 2002. The economic effects of harmful algal blooms in the United States: Estimates, assessment issues, and information needs. Estuaries 25, 819-837.

Jean, N., Bogé, G., Jamet, J.-L., Richard, S., Jamet, D., 2005. Annual contribution of different plankton size classes to particulate dimethylsulfoniopropionate in a marine perturbed ecosystem. J. Mar. Syst. 53, 235-247.

Jean, N., Dumont, E., Durrieu, G., Balliau, T., Jamet, J.-L., Personnic, S., Garnier, C., 2012. Protein expression from zooplankton communities in a metal contaminated NW mediterranean coastal ecosystem. Mar. Environ. Res. 80, 12-26.

Jean, N., Dumont, E., Herzi, F., Balliau, T., Laabir, M., Masseret, E., Mounier, S., 2017. Modifications of the soluble proteome of a mediterranean strain of the invasive neurotoxic dinoflagellate *Alexandrium catenella* under metal stress conditions. Aquat. Toxicol. 188, 80-91.

Jiang, X.-W., Wang, J., Gao, Y., Chan, L.L., Lam, P.K.S., Ju, J.-D., 2015. Relationship of proteomic variation and toxin synthesis in the dinoflagellate *Alexandrium tamarense* CI01 under phosphorus and inorganic nitrogen limitation. Ecotoxicology 24, 1744-1753.

Kao, C.Y., Walker, S.E., 1982. Active groups of saxitoxin and tetrodotoxin as deduced from actions of saxitoxin analoguew on frog muscle and squid axon. J. Physiol. 323, 619-637.

Khatiwada, B., Hasan, M.T., Sun, A., Kamath, K.S., Mirzaei, M., Sunna, A., Nevalainen, H., 2020. Proteomic response of *Euglena gracilis* to heavy metal exposure - identification of key proteins involved in heavy metal tolerance and accumulation. Algal Res. 45, 101764.

Kim, Y.K., Yoo, W.I., Lee, S.H., Lee, M.Y., 2005. Proteomic analysis of cadmium-induced protein profile alterations from marine alga *Nannochloropsis oculata*. Ecotoxicology 14, 589-596.

Kong, L., Price, N.M., 2020. Identification of copper-regulated proteins in an oceanic diatom, *Thalassiosira oceanica* 1005. Metallomics 12, 1106-1117.

Krock, B., Seguel, C.G., Cembella, A.D., 2007. Toxin profile of *Alexandrium catenella* from the Chilean coast as determined by liquid chromatography with fluorescence detection and liquid chromatography coupled with tandem mass spectrometry. Harmful Algae 6, 734-744.

Laabir, M., Jauzein, C., Genovesi, B., Masseret, E., Grzebyk, D., Cecchi, P., Vaquer, A., Perrin, Y., Collos, Y., 2011. Influence of temperature, salinity and irradiance on the growth and cell yield of the harmful red tide dinoflagellate *Alexandrium catenella* colonising Mediterranean waters. J. Plankton Res. 22, 1550-1563.

Laabir, M., Collos, Y., Masseret, E., Grzebyk, D., Abadie, E., Savart, V., Sibat, M., Amzil, Z., 2013. Influence of environmental factors on the paralytic shellfish toxin content and profile of *Alexandrium pacificum* (Dinophyceae) isolated from the Mediterranean Sea. Mar. Drugs 11, 1583-1601.

Laemmli, K., 1970. Cleavage of structural proteins during the assembly of the bacteriophage T4. Nature 227, 680-685.

Langella, O., Valot, B., Balliau, T., Blein-Nicolas, M., Bonhomme, L., 2017. X!TandemPipeline: a tool to manage sequence redundancy for protein inference and phosphosite identification. J. Proteome Res. 2, 494-503.

Le, Q.H., Markovic, P., Hastings, J.W., Jovine, R.V.M., Morse, D., 1997. Structure and organization of the peridinin-chlorophyll *a*-binding protein gene in *Gonyaulax polyedra*. Mol. Gen. Genet. 255, 595-604.

Leon-Vaz, A., Romero, L.C., Gotor, C., Leon, R., Vigara, J., 2021. Effect of cadmium in the microalga *Chlorella sorokiniana*: a proteomic study. Ecotox. Environ. Safe. 207, 111301.

Linares, D., Jean, N., Van Overtvelt, P., Ouisse, T., Hardouin, J., Blache, Y., Molmeret, M., 2016. The marine bacteria *Shewanella frigidimarina* NCIMB400 up regulates the type VI secretion system during early biofilm formation. Environ. Microbiol. Rep. 8, 110-121.

Lowry, O.H., Rosebrough, N.J., Farr, A.L., Randall, R.J., 1951. Protein measurement with the Folin phenol reagent. J. Biol. Chem. 193, 265-275.

Luglié, A., Sechi, N., Oggiano, G., Sanna, G., Tapparo, A., 2002. Ecological assessment of Santa Giusta Lagoon (Sardinia, Italy). Ann. Chim. 92, 239-247.

Margalef, R., Estrada, M., 1987. Synoptic distribution of summer microplankton (Algae and Protozoa) across the principal front in the Western Mediterranean. Inv. Pesq. 51(1), 121-140.

Marzano, V., Santini, S., Rossi, C., Zucchelli, M., D'Alessandro, A., Marchetti, C., Mingardi, M., Stagni, V., Barila, D., Urbani, A., 2012. Proteomic profiling of ATM kinase proficient and deficient cell lines upon blockage of proteasome activity. J. Proteomics 75, 4632-4646.

Okamoto, O.K., Colepicolo, P., 1998. Response of superoxide dismutase to pollutant metal stress in the marine dinoflagellate *Gonyaulax polyedra*. Comp. Biochem. Physiol. Part C: Pharmacol. Toxicol. Endocrinol. 119, 67-73.

Park, T.G., Lim, W.A., Park, Y.T., Lee, C.K., Jeong, H.J., 2013. Economic impact, management and mitigation of red tides in Korea. Harmful Algae, Red Tides in Korea 30, S131–S143.

Penna, A., Garcès, E., Vila, M., Giacobbe, M.G., Fraga, S., Lugliè, A., Bravo, I., Bertozzini, E., Vernesi, C., 2005. *Alexandrium catenella* (Dinophyceae), a toxic ribotype expanding in the NW Mediterranean Sea. Mar. Biol. 148, 13-23.

Pinedo, S., Jordana, E., Flagella, M.M., Ballesteros, E., 2014. Relationships between heavy metals contamination in shallow marine sediments with industrial and urban development in Catalonia (Northwestern Mediterranean Sea). Water Air. Soil Pollut. 225, 2084-3000.

Quod, J.P., Turquet, J., 1996. Ciguatera in Réunion Island (SW Indian Ocean): epidemiology and clinical patterns. Toxicon 34, 779-785.

Rabilloud, T., Lelong, C., 2021. The whereabouts of 2D gels in quantitative proteomics. Methods Mol Biol 2228, 41-51.

Reumann, S., Weber, A.P.M., 2006. Plant peroxisomes respire in the light: some gaps of the photorespiratory C2 cycle have become filled-others remain. Biochim. Biophys. Acta-Mol. Cell Res. 1763, 1496-1510.

Rhodes, L., Selwood, A., McNabb, P., Briggs, L., Adamson, J., van Ginkel, R., Laczka, O., 2006. Trace metal effects on the production of biotoxins by microalgae. Afr. J. Aquat. Sci. 28, 393-397.

Ritter, A., Ubertini, M., Romac, S., Gaillard, F., Delage, L., Mann, A., Cock, J.M., Tonon, T., Correa, J.A., Potin, P., 2010. Copper stress proteomics highlights local adaptation of two strains of the model brown alga *Ectocarpus siliculosus*. Proteomics 10, 2074-2088.

Savela, H., Harju, K., Spoof, L., Lindehoff, E., Merluoto, J., Vieniainen, M., Kremp, A., 2016. Quantity of the dinoflagellate stxA4 gene and cell density correlates with paralytic shellfish toxin production in *Alexandrium ostenfeldii* blooms. Harmful Algae 52, 1-10.

Schuback, N., Hippmann, A., Maldonado, M.T., Allen, A.E., McCrow, J., Foster, L.J., Green, B.R., Alami, M., 2016. Constrasting physiological and proteomic adaptations to iron

and/or copper limitation in two strains of the same open ocean diatom *Thalassiosira oceanica*. Proteomics 10, 2074-2088.

Selander, E., Thor, P., Toth, G., Pavia, H., 2006. Copepods induce paralytic shellfish toxin production in marine dinoflagellates. Proc. R. Soc. B. 273, 1673-1680.

Siano, R., Lassudrie, M., Cuzin, P., Briant, N., Loizeau, V., Schmidt, S., Ehrhold, A., Mertens, K.N., Lambert, C., Quintric, L., Noel, C., Latimier, M., Quéré, J., Durand, P., Penaud, A., 2021 (in press). Sediment archives reveal irreversible shifts in plankton communities after World War II and agricultural pollution. Curr. Biol., https://doi.org/10.1016/j.cub.2021.03.079.

Tessier, E., Garnier, C., Mullot, J.-U., Lenoble, V., Arnaud, M., Raynaud, M., Mounier, S., 2011. Study of the spatial and historical distribution of sediment inorganic contamination in the Toulon bay (France). Mar. Pollut. Bull. 62, 2075-2086.

Tripathi, S., Poluri, K.M., 2021 Heavy metal detoxification mechanisms by microalgae: Insights from transcriptomics analysis. Environ. Poll. 285, 117443.

Tse, S.P., Lee, F.W., Mak, D.Y., Kong, H., Chan, K.K., Lo, P., Lo, S., 2020. Production of paralytic shellfish toxins (PSTs) in toxic *Alexandrium catenella* is intertwined with photosynthesis and energy production. Toxins 12, 477.

Van de Riet, J.M., Gibbs, R.S., Chou, F.W., Muggah, P.M., Rourke, W.A., Burns, G., Thomas, K., Quilliam, M.A., 2009. Liquid chromatographic post-column oxidation method for analysis of Paralytic Shellfish Toxins in mussels, clams, scallops, and oysters: single-laboratory validation. J. AOAC Int. 92, 1690-1704.

Wang, D.-Z., Gao, Y., Lin, L., Hong, H.S., 2013. Comparative proteomic analysis reveals proteins putatively involved in toxin biosynthesis in the marine dinoflagellate *Alexandrium catenella*. Mar. Drugs 11, 213-232.

Wang, D.-Z., Li, C., Zhang, Y., Wang, Y.Y., He, Z.P., Lin, L., Hong, H.S., 2012. Quantitative proteomic analysis of differentially expressed proteins in the toxicity-lost mutant of *Alexandrium catenella* (Dinophyceae) in the exponential phase. J. Prot. 75, 5564-5577.

Wang, D.-Z., Lin, L., Gu, H.-F., Chan, L.L., Hong, H.-S., 2008. Comparative studies on morphology, ITS sequence and protein profile of *Alexandrium tamarense* and *A. pacificum* isolated from the China Sea. Harmful Algae 7, 106-113.

Wera, S., Hemmings, B.A., 1995. Serine/threonine protein phosphatases. Biochem. J. 311, 17-29.

Zhan, X., Li, B., Zhan, X., Schlüter, H., Jungblut, P.R., Coorssen, J.R., 2021. A review on innovating the concept and practice of two-dimensional gel electrophoresis in the analysis of proteomes at the proteoform level. Curr. Adv. Chem. Biochem. 2, 135-152.

Zhang, S.-F., Zhang, Y., Lin, L., Wang, D.-Z., 2018. iTRAQ-based quantitative proteomic analysis of a toxigenic dinoflagellate *Alexandrium catenella* at different stages of toxin biosynthesis during the cell cycle. Mar. Drugs 16, 491.

Zhang, Y., Zhang, S.-F., Lin, L., Wang, D.-Z., 2014. Comparative transcriptome analysis of a toxin-producing dinoflagellate *Alexandrium catenella* and its non-toxic mutant. Mar. Drugs 12, 5698-5718.

Zou, H.X., Pang, Q.Y., Zhang, A.Q., Lin, L.D., Li, N., Yan, X.-F., 2015. Excess copper induced proteomic changes in the marine brown alga *Sargassum fusiforme*. Ecotox. Environ. Safe. 111, 271-280.

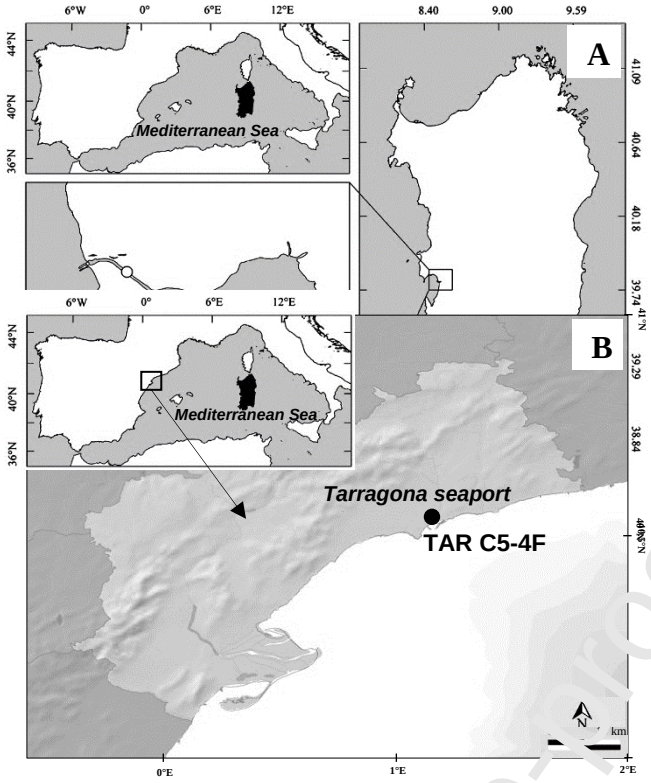

Figure 1

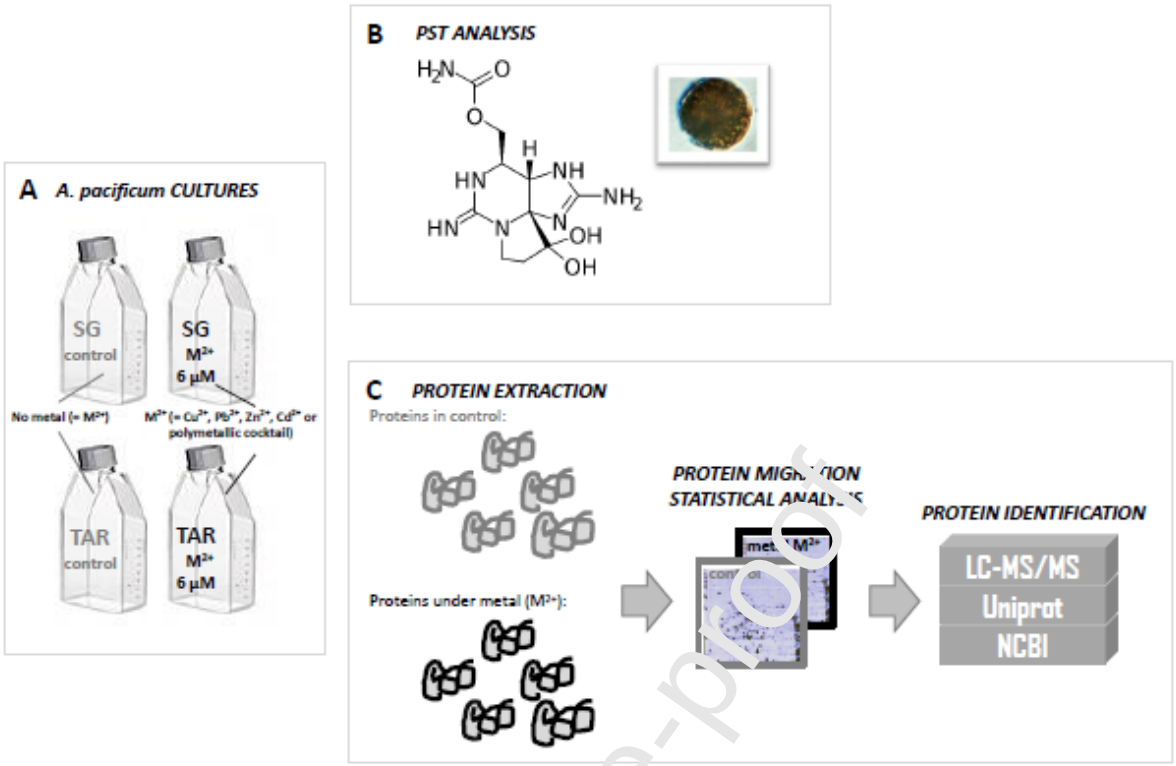

Figure 2

A

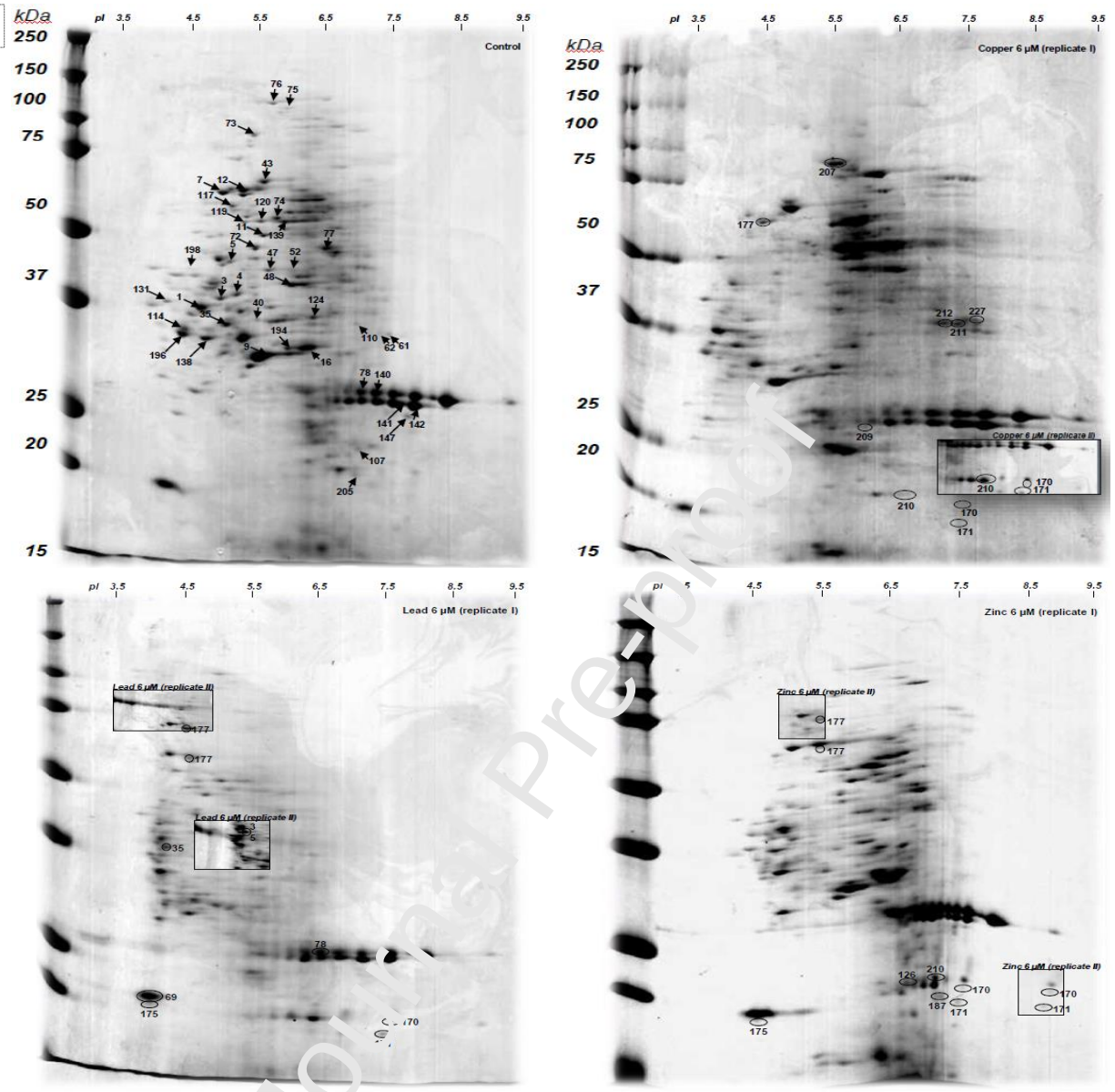

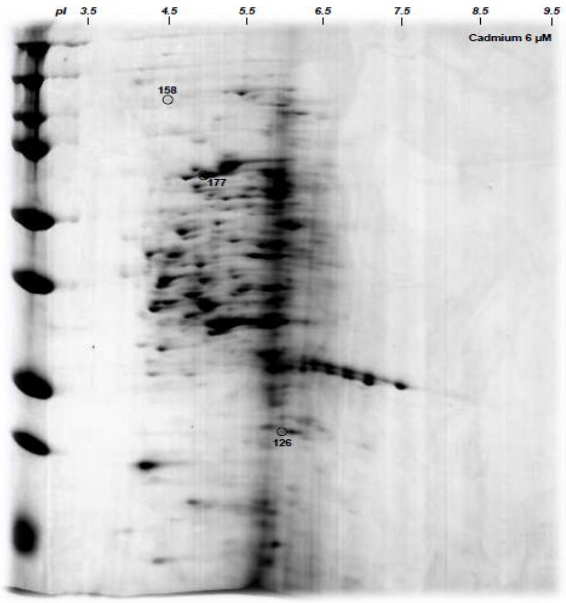

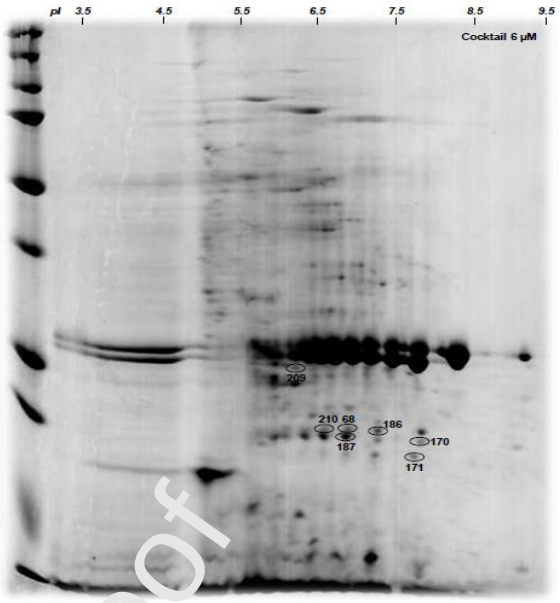

Spot	Protein Name	*Copper 6 µM*	*Lead 6 µM*	*Zinc 6 µM*	*Cadmium 6 µM*	*Cocktail 6 µM*
1	Glyceraldehyde-3-phosphate dehydrogenase					-3.7**
3	Unidentified protein					-2.2*
4	Unidentified protein	**D**		-5.5**		-4.4**
5	Unidentified protein	**D**		-3.3**	-3.9**	-2.7*
7	Unidentified protein	-3.4**		-2.1**		-2.4**
9	Unidentified protein			-4.7**		-13.1**
11	Unidentified protein	-3.7**		-2.1*	-2.6**	-2.4*
12	Unidentified protein	-5.3**	-3.5**		-5.2**	-5.5**
16	Serine carboxypeptidase	-3.1**				-4.1*
35	Unidentified protein	**D**	+2.7**			**D**
40	Chloroplast ferredoxin-NADP(+) reductase	**D**				**D**
43	WSC domain-containing protein					**D**
47	Ribulose bisphosphate carboxylase		**D**			**D**
48	Copper/zinc superoxide dismutase	-5.7**	-3.3**	-3.8*		**D**
52	Probable high CO_2 inducible periplasmic protein				**D**	**D**
61	Chloroplast ferredoxin-NADP(+) reductase			**D**		**D**
62	Chloroplast ferredoxin-NADP(+) reductase					**D**
68	Peridinin chlorophyll-*a* binding protein					+8.4*
69	Unidentified protein		+2.7***			
72	Unidentified protein		-3.7***	-3.0**		
73	Unidentified protein	-3.9**	-9.0***	-6.5**	-4.7**	
74	Heat shock protein 60		-2.6*		-3.2*	
75	Unidentified protein		-3.4*			
76	Unidentified protein		-5.6**			
77	Catalase peroxidase		-3.1*	-2.2**	-2.4*	
78	Peridinin chlorophyll-*a* binding protein		+2.9*			
107	Ribulose bisphosphate carboxylase		**D**			
110	Chloroplast ferredoxin-NADP(+) reductase	**D**	**D**		-4.0*	
114	Chloroplast ferredoxin-NADP(+) reductase	**D**		-5.2*		
117	Unidentified protein			-3.8**		
119	Ribulose bisphosphate carboxylase			-2.2**	-2.9**	
120	Unidentified protein	-2.6**		-4.1**		
124	Adenosine kinase			-2.2*		
126	Peridinin chlorophyll-*a* binding protein			+11.3**	+3.7*	
131	Glyceraldehyde-3-phosphate dehydrogenase	**D**		**D**	-4.6***	
138	Unidentified protein	-11.7***			-4.6***	
139	ATP synthase subunit				-5.9*	
140	Proteasome subunit				-2.0**	
141	Peridinin chlorophyll-*a* binding protein				-5.4**	
142	Peridinin chlorophyll-*a* binding protein				-3.3*	
147	Proteasome subunit				**D**	
158	Unidentified protein				**A**	
170	Peridinin chlorophyll-*a* binding protein	**A**	**A**	**A**		**A**
171	Peridinin chlorophyll-*a* binding protein	**A**	**A**	**A**		**A**

175	Copper/zinc superoxide dismutase		**A**	**A**		
177	Heat shock protein 60	**A**	**A**	**A**	**A**	
186	Peridinin chlorophyll-*a* binding protein					**A**
187	Peridinin chlorophyll-*a* binding protein			**A**		**A**
194	Serine carboxypeptidase	-3.1**				
196	Unidentified protein	**D**				
198	Unidentified protein	**D**				
205	Peridinin chlorophyll-*a* binding protein	**D**				
207	Phosphoenolpyruvate synthase	**A**				
209	Proteasome subunit	**A**				**A**
210	Peridinin chlorophyll-*a* binding protein	**A**		**A**		**A**
211	Chloroplast ferredoxin-NADP(+) reductase	**A**				
212	Glyceraldehyde-3-phosphate dehydrogenase	**A**				
227	Glyceraldehyde-3-phosphate dehydrogenase	**A**				

Figure 3

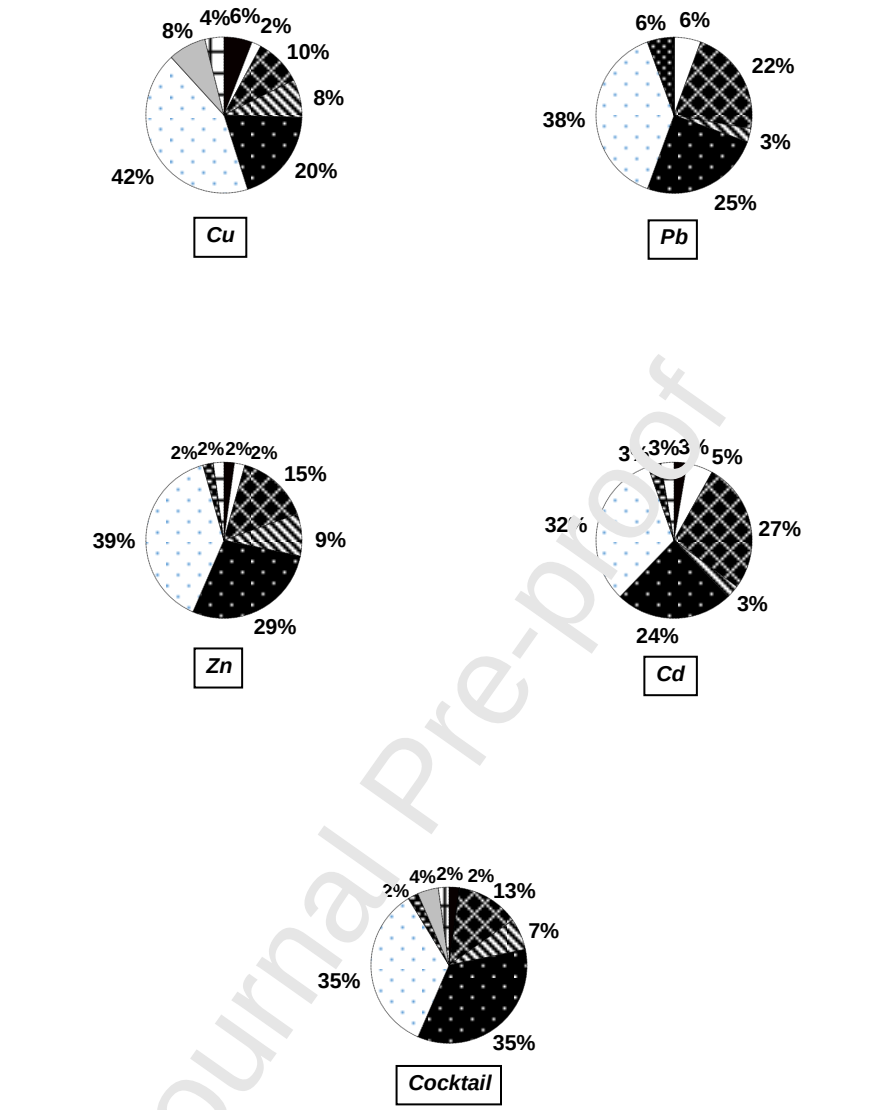

Figure 4

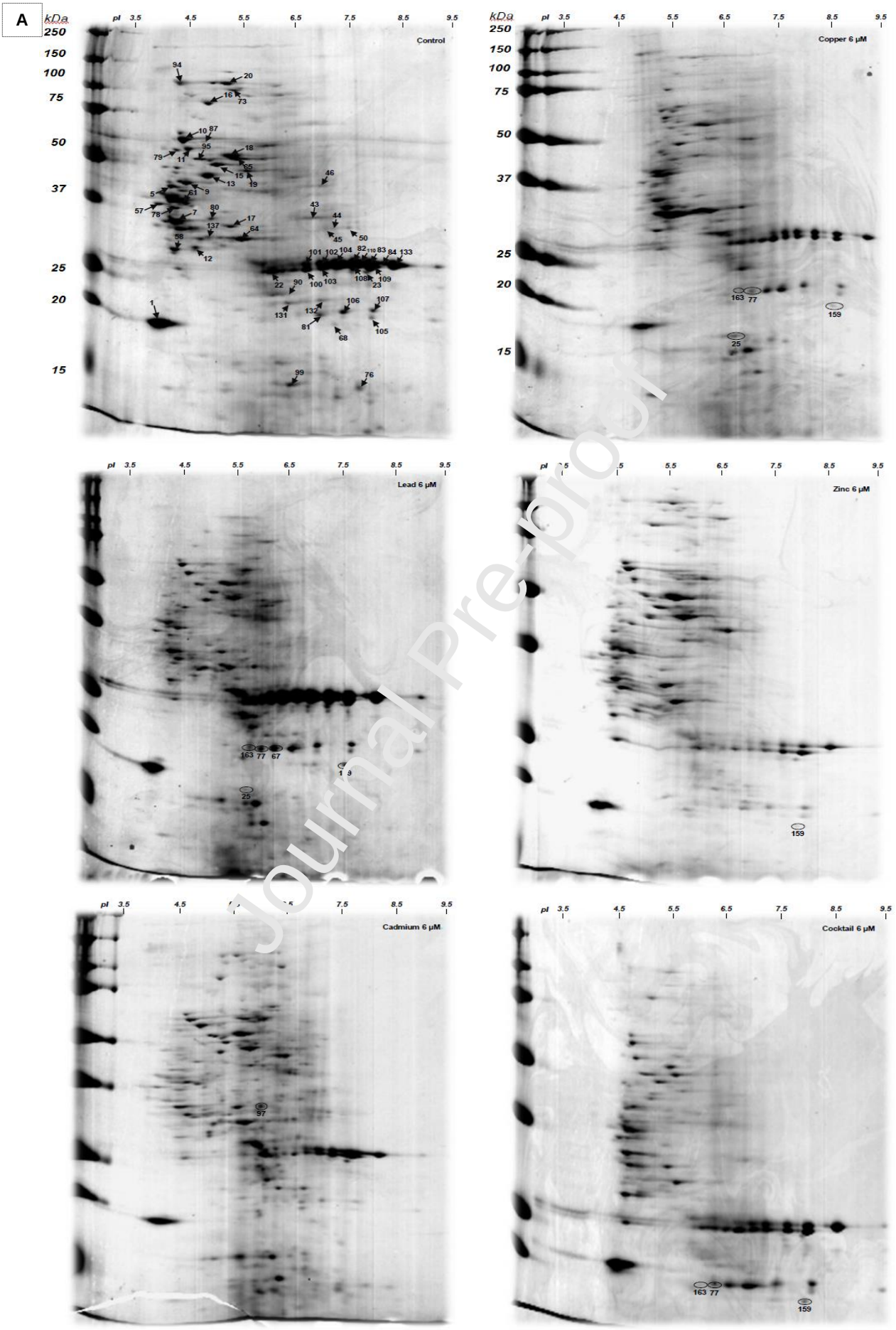

B

Spot	Protein Name	*Copper 6 µM*	*Lead 6 µM*	*Zinc 6 µM*	*Cadmium 6 µM*	*Cocktail 6 µM*
1	Unidentified protein	-3.8***			-6.0***	-2.2***
5	Unidentified protein	-6.6**	-2.8**		-9.3**	-3.9***
7	Unknown protein	-2.6**	-2.7***	-2.6**	-6.2***	-2.6***
9	Unidentified protein	-5.1*	-2.9*		-6.0*	-3.8**
10	Unidentified protein	-11.7***	-2.3**	-2.6***	-5.5***	-4.7***
11	Unidentified protein	-2.4*		-2.5**	-3.1*	-2.7***
12	Peridinin chlorophyll-*a* binding protein	-5.8***	-5.0***		-2.7**	
13	Unidentified protein	-3.8***	-3.4***	-2.5*	-2.6**	-4.4***
15	Unidentified protein	-8.9**	-2.9**		-4.1**	-2.8***
16	Unidentified protein	-3.0*	-2.3*	-2.0*	-4.1**	-2.1**
17	Translation initiation inhibitor	-4.6***	-3.1**			
18	Adenylosuccinate synthetase	-2.8*	-2.5*		-3.1*	
19	Unknown protein	-5.0**				-2.1*
20	Unidentified protein	-7.6***	-3.8**	-4.2***	-2.6*	-6.9***
22	Heat shock protein 70	-2.6*		-2.3**	-2.9**	-3.2***
23	Proteasome subunit	-43.7*				-6.7**
25	Serine/threonine-protein phosphatase	**A**	**A**			
43	Chloroplast ferredoxin-NADP(+) reductase	**D**				-4.1*
44	Chloroplast ferredoxin-NADP(+) reductase	**D**				**D**
45	Chloroplast ferredoxin-NADP(+) reductase	**D**				**D**
46	Ribulose bisphosphate carboxylase	**D**				**D**
50	Chloroplast ferredoxin-NADP(+) reductase	**D**				**D**
57	Unidentified protein		-3.7***	-2.4*	-5.6***	-2.0**
58	Unidentified protein		-2.8***	-2.1*	-5.6***	
61	Agmatinase		-3.2***	-8.6**	-7.0***	-2.9***
64	Serine/threonine-protein phosphatase		-2.5**	-3.4***	-2.9***	-2.6***
65	ATP synthase subunit		-2.[illegible]	-2.5*	-3.2***	
67	Peridinin chlorophyll-*a* binding protein		+[illegible]1***			
68	Calreticulin		-3.4*		**D**	-4.6***
73	Unidentified protein		**D**	-6.4***	-5.3**	-6.5***
76	Luciferin Binding Protein		**D**		**D**	
77	Peridinin chlorophyll-*a* binding protein	**A**	**A**			**A**
78	Methionine S-adenosyl transferase		-2.0**		-4.0***	
79	Unknown protein		-3.4*	+11.3**	-3.6*	-5.8**
80	Chloroplast ferredoxin-NADP(+) reductase			-5.0***	-4.3**	
81	Peridinin chlorophyll-*a* binding protein			-2.8*		
82	Peridinin chlorophyll-*a* binding protein			-3.4*	-10.6**	-2.7**
83	Peridinin chlorophyll-*a* binding protein			-3.8*	-10.5*	-4.4**
84	Peridinin chlorophyll-*a* binding protein			-6.0**	-4.1*	
87	Unidentified protein			**D**		
90	Ribulose bisphosphate carboxylase			**D**		
94	Unidentified protein				-25.2**	-13.8**
95	Leucine aminopeptidase				-5.3*	
97	Adenosine kinase				+3.0**	
99	Protein kinase C conserved region 2				-3.3*	
100	Peridinin chlorophyll-*a* binding protein				-6.5**	-2.2**
101	Peridinin chlorophyll-*a* binding protein				-30.0**	
102	Peridinin chlorophyll-*a* binding protein				-11.1**	
103	Peridinin chlorophyll-*a* binding protein				-6.5***	
104	Proteasome subunit				-14.8***	-2.5*
105	Peridinin chlorophyll-*a* binding protein				-6.4*	
106	Peridinin chlorophyll-*a* binding protein				-4.0***	
107	Peridinin chlorophyll-*a* binding protein				-3.8***	
108	Proteasome subunit				-3.9**	
109	Peridinin chlorophyll-*a* binding protein				-3.9**	
110	Peridinin chlorophyll-*a* binding protein				-6.4**	-4.8**
131	Proteasome subunit					-4.2**
132	Ribulose bisphosphate carboxylase					-8.6**
133	Peridinin chlorophyll-*a* binding protein					-4.9*
137	Unidentified protein					**D**
159	Peridinin chlorophyll-*a* binding protein	**A**	**A**	**A**		**A**
163	Heat shock protein 70	**A**	**A**			**A**

Figure 5

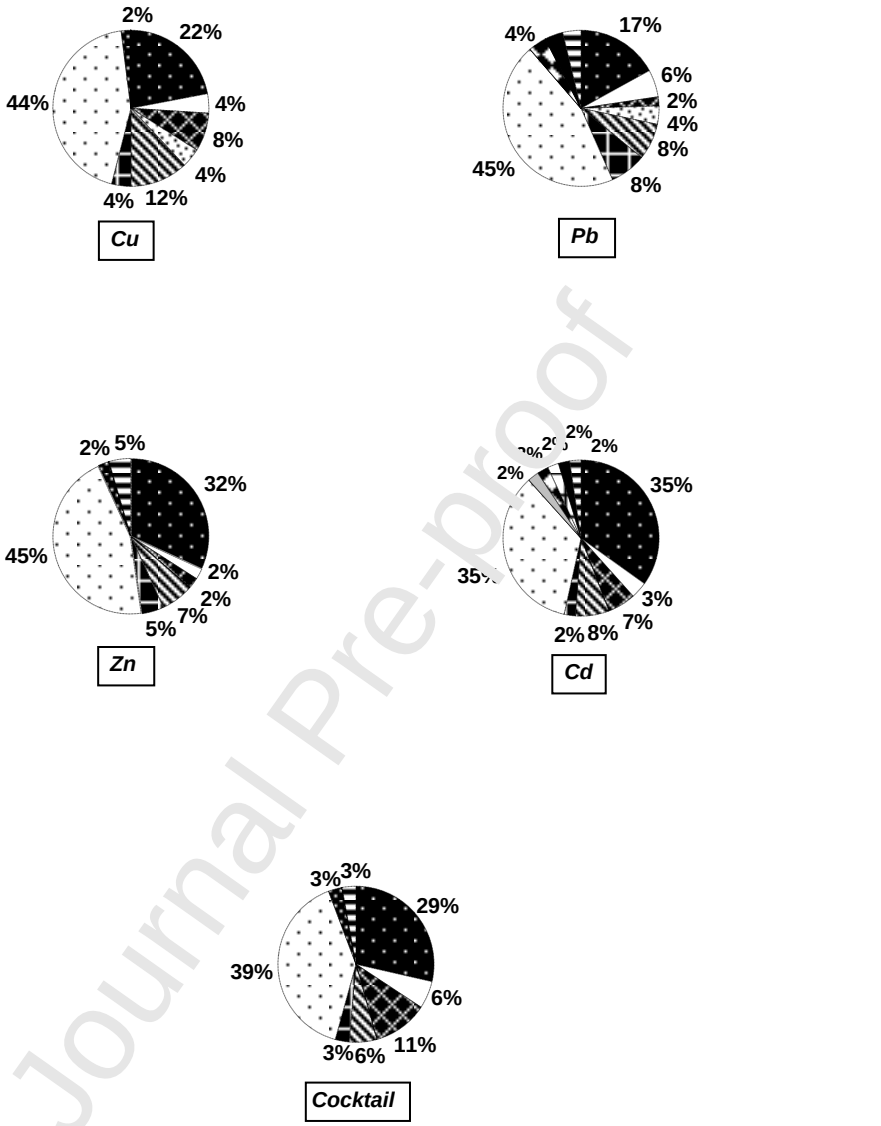

Figure 6

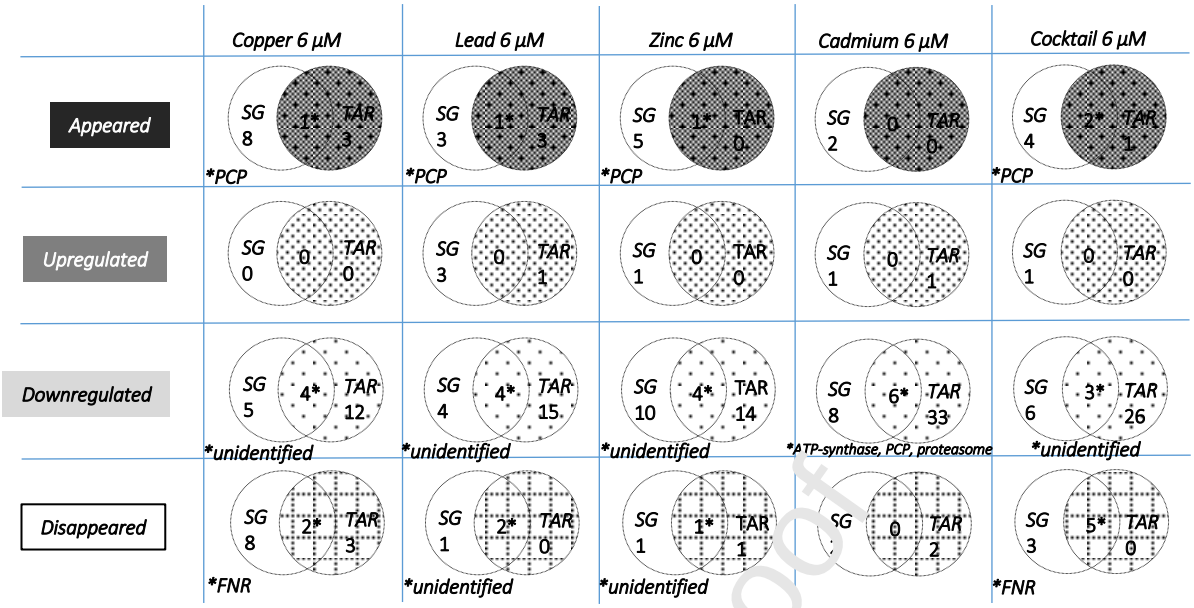

Figure 7

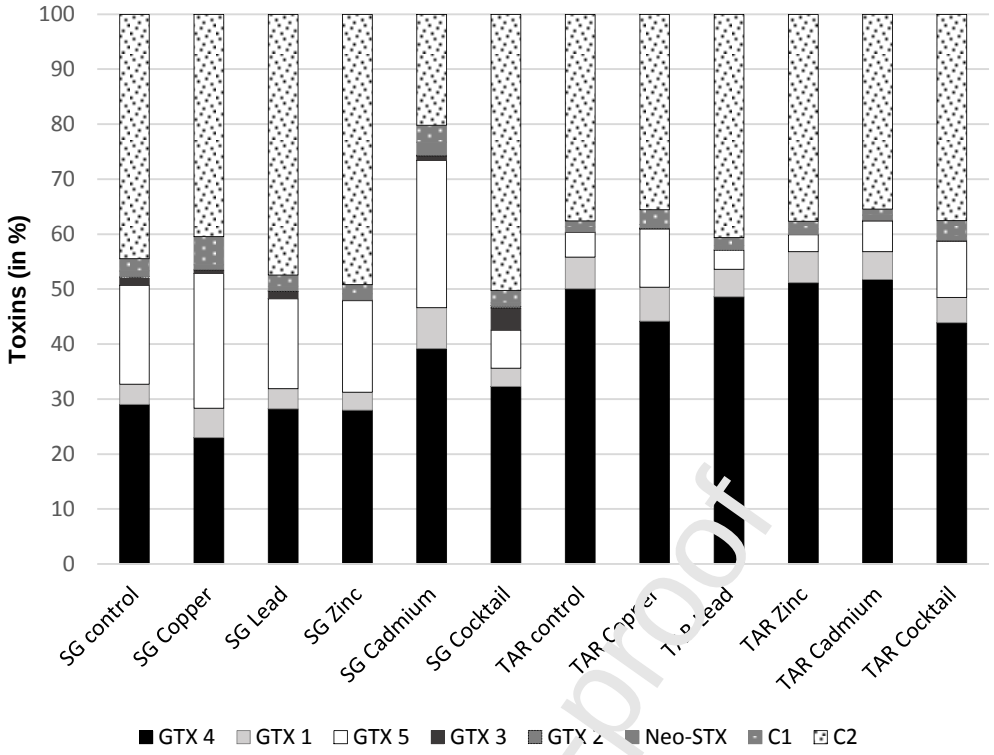

Figure 8

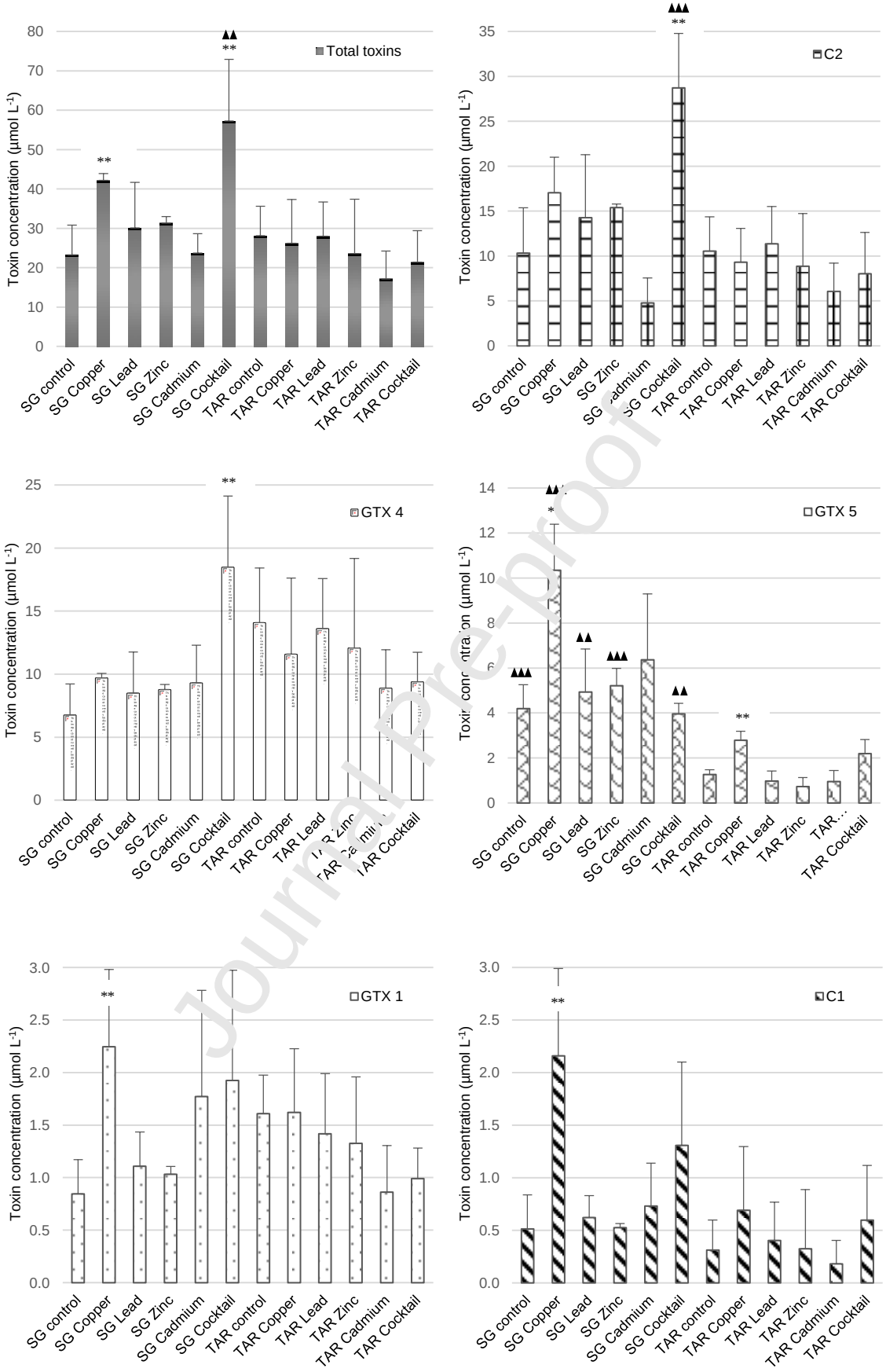

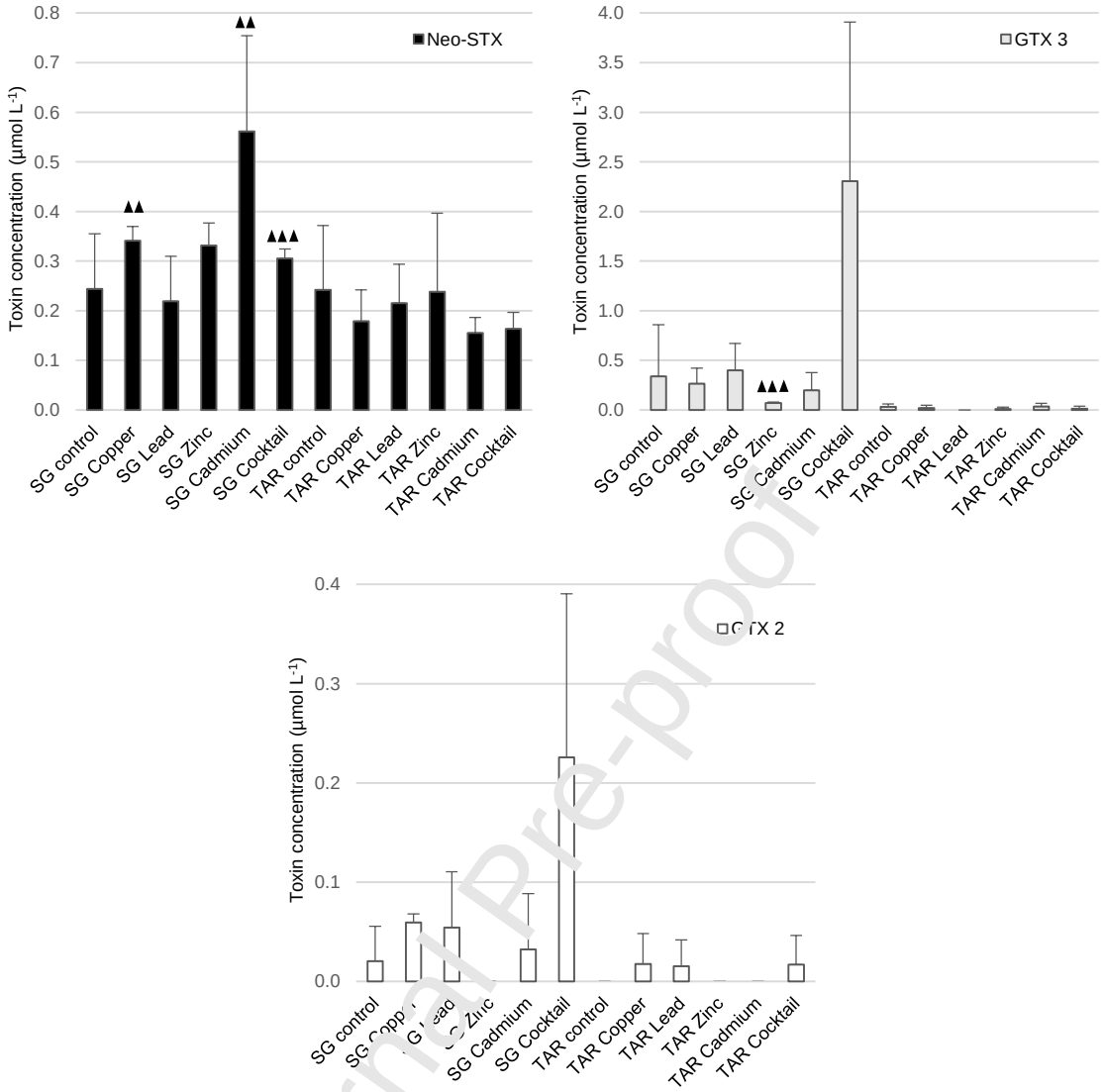

Figure 9

Table 1

Spot	Peptide number	MW (kDa) / pI		Protein name	Species Accession number	Putative function
		Exp	Theo			
124	4	34.3/5.5	37.6/6.0	Adenosine kinase	*Symbiodinium microadriaticum* OLQ033971	Purine nucleoside anabolism (01.03.01.03)
139	3	51.4/5.1	60.0/6.4	ATP synthase subunit	*Neospora caninum* F0VGD5	Energy generation (02.45.15)
77	6	45.5/5.6	74.4/5.2	Catalase peroxidase	*Phytophthora infestans* XP002905104	Catalase reaction (32.07.07.01)
40	8	34.0/4.9	45.0/7.0	Chloroplast ferredoxin-NADP(+) reductase	*Heterocapsa triquetra* AAW79314	Electron transport (20.01.15)
61	17	32.2/6.3	45.0/7.0	Chloroplast ferredoxin-NADP(+) reductase	*Crypthecodinium cohnii* Q5ENS9	Electron transport (20.01.15)
62	19	32.2/6.2	45.0/7.0	Chloroplast ferredoxin-NADP(+) reductase	*Heterocapsa triquetra* Q5ENS9	Electron transport (20.01.15)
110	23	33.5/6.0	45.0/7.0	Chloroplast ferredoxin-NADP(+) reductase	*Heterocapsa triquetra* Q5ENS9	Electron transport (20.01.15)
114	2	32.9/4.1	45.0/7.0	Chloroplast ferredoxin-NADP(+) reductase	*Heterocapsa triquetra* AAW79314	Electron transport (20.01.15)
211	12	36.5/6.2	45.0/7.0	Chloroplast ferredoxin-NADP(+) reductase	*Heterocapsa triquetra* AAW79314	Electron transport (20.01.15)
48	3	38.9/5.3	17.0/5.2	Copper/zinc superoxide dismutase	*Ulva fasciata* ABB88583	Superoxide reaction (32.07.7.7)
175	2	10.8/3.8	17.0/5.2	Copper/zinc superoxide dismutase	*Ulva fasciata* ABB88583	Superoxide reaction (32.07.07.07)
1	2	35.5/4.3	36.6/5.9	Glyceraldehyde-3-phosphate dehydrogenase	*Alexandrium fundyense* ABO47862	Glycolysis (02.01)
131	2	36.4/3.9	36.6/5.9	Glyceraldehyde-3-phosphate dehydrogenase	*Alexandrium fundyense* ABO47862	Glycolysis (02.01)
212	14	36.6/6.1	36.6/5.9	Glyceraldehyde-3-phosphate dehydrogenase	*Alexandrium fundyense* ABO47862	Glycolysis (02.01)
227	17	37.1/6.4	36.6/5.9	Glyceraldehyde-3-phosphate dehydrogenase	*Alexandrium fundyense* ABO47862	Glycolysis (02.01)
74	2	52.3/5.1	59.5/5.2	Heat shock protein 60	*Perkinsus marinus* XP002785716	Chaperone (14.01)
177	3	58.8/4.7	59.5/5.2	Heat shock protein 60	*Perkinsus marinus* XP002785716	Chaperone (14.01)
68	16	13.2/6.3	38.0/9.1	Peridinin chlorophyll-a binding protein	*Symbiodinium* sp. AFH8837	Light absorption (02.45.03)
78	7	26.1/6.0	38.0/9.1	Peridinin-chlorophyll a-binding protein	*Symbiodinium* sp. AFH88375	Light absorption (02.45.03)
126	7	13.3/5.6	38.0/9.1	Peridinin chlorophyll-a binding protein	*Symbiodinium* sp. AFH88375	Light absorption (02.45.03)
141	15	25.0/6.4	38.0/9.1	Peridinin chlorophyll-a binding protein	*Symbiodinium* sp. AFH88375	Light absorption (02.45.03)
142	18	24.2/6.6	38.9/9.0	Peridinin-chlorophyll *a*-binding protein	*Glenodinium polyedra* O00841	Light absorption (02.45.03)
170	16	11.6/6.6	38.0/9.1	Peridinin chlorophyll-a binding protein	*Symbiodinium* sp. AFH88375	Light absorption (02.45.03)
171	12	10.2/6.5	38.0/9.1	Peridinin chlorophyll-a binding protein	*Symbiodinium* sp. AFH88375	Light absorption (02.45.03)
186	9	13.2/6.4	38.0/9.1	Peridinin chlorophyll-a binding protein	*Symbiodinium* sp. AFH88375	Light absorption (02.45.03)
187	9	12.6/6.3	38.0/9.1	Peridinin chlorophyll-a binding protein	*Symbiodinium* sp. AFH88375	Light absorption (02.45.03)
205	10	12.6/5.9	38.0/9.1	Peridinin chlorophyll-a binding protein	*Symbiodinium* sp. AFH88375	Light absorption (02.45.03)
210	15	13.4/5.9	38.0/9.1	Peridinin chlorophyll-a binding protein	*Symbiodinium* sp. AFH88375	Light absorption (02.45.03)
207	35	78.8/5.4	partial	Phosphoenolpyruvate synthase, partial	*Symbiodinium microadriaticum* OLP73462	Gluconeogenesis (02.01)
52	5	40.8/5.3	partial	Probable high CO_2 inducible periplasmic protein	*Heterocapsa triquetra* AAW79380	Gas and metabolite distribution (34.11.13)
107	4	16.1/6.0	22.6/6.1	Proteasome subunit	*Daphnia magna* JAN48661	Proteasomal degradation (14.13.01.01)
140	8	26.0/6.2	27.9/5.8	Proteasome subunit	*Alexandrium fundyense* A4UHA5	Proteasomal degradation (14.13.01.01)
147	9	22.2/6.5	27.5/5.2	Proteasome subunit	*Perkinsus marinus* EER11732	Proteasomal degradation (14.13.01.01)
209	2	23.9/5.8	29.0/5.4	Proteasome alpha subunit	*Perkinsus marinus* XP_002775560	Proteasomal degradation (14.13.01.01)
47	2	41.4/5.0	164.4/5.7	Ribulose bisphosphate carboxylase	*Symbiodinium* sp. AAB17550	Photosynthesis (02.30)
119	3	51.3/4.7	56.1/5.6	Ribulose bisphosphate carboxylase	*Symbiodinium* sp. AAB17550	Photosynthesis (02.30)
16	7	30.7/5.4	95.6/4.9	Serine carboxypeptidase	*Symbiodinium microadriaticum* OLP90538	Protein degradation (14.13)
194	3	30.6/5.2	95.6/4.9	Serine carboxypeptidase	*Symbiodinium microadriaticum* OLP90538	Protein degradation (14.13)
43	3	63.1/5.0	partial	WSC domain-containing protein	*Marssonina brunnea* XP007294042	Unclassified protein (99)

Table 2

Spot	Peptide number	MW (kDa) / pI		Protein name	Species Accession number	Putative function
		Exp	Theo			
97	4	32.6/6.2	37.6/6.0	Adenosine kinase	*Symbiodinium microadriaticum* OLQ033971	Purine nucleoside anabolism (01.03.01.03)
18	3	52.1/5.1	49.4/5.4	Adenylosuccinate synthetase	*Perkinsus marinus* EER05541	Purine nucleotide anabolism (01.03.01.03)
61	5	37.7/4.6	45.3/5.5	Agmatinase	*Phaeodactylum tricornutum* EEC43644	Metabolism of urea (01.01.05.03)
65	3	52.0/5.6	60.0/6.4	ATP synthase subunit	*Neospora caninum* F0VGD5	Energy generation (02.45.15)
68	10	18.3/6.6	27.2/5.0	Calreticulin	*Heterocapsa triquetra* Q5ENL5	Calcium binding (16.17.01)
43	2	32.5/5.9	45.0/7.0	Chloroplast ferredoxin-NADP(+) reductase	*Heterocapsa triquetra* Q5ENS9	Electron transport (20.01.15)
44	19	30.6/6.5	45.0/7.0	Chloroplast ferredoxin-NADP(+) reductase	*Heterocapsa triquetra* Q5ENS9	Electron transport (20.01.15)
45	23	30.5/6.1	45.0/7.0	Chloroplast ferredoxin-NADP(+) reductase	*Heterocapsa triquetra* Q5ENS9	Electron transport (20.01.15)
50	17	30.7/6.4	45.0/7.0	Chloroplast ferredoxin-NADP(+) reductase	*Crypthecodinium cohnii* Q5ENS9	Electron transport (20.01.15)
80	8	33.9/5.4	45.0/7.0	Chloroplast ferredoxin-NADP(+) reductase	*Heterocapsa triquetra* AAW79314	Electron transport (20.01.15)
22	11	26.2/5.8	74.3/5.1	Heat shock protein 70	*Crypthecodinium cohnii* Q8S4R0	Chaperone (16.21.01)
163	2	19.0/5.4	70.6/5.1	Heat shock protein 70	*Crypthecodinium cohnii* Q8S4Q8	Chaperone (16.21.01)
7	16	32.5/4.3	50.3/5.1	Hypothetical protein	*Plasmodium berghei* Q4YAV6	Unclassified protein (99)
79	5	53.7/4.3	45.6/5.6	Hypothetical protein	*Caenorhabditis remanei* EFO94103	Unclassified protein (99)
95	2	51.2/5.2	54.5/5.7	Leucine aminopeptidase	*Arabidopsis thaliana* P30184	Protein degradation (14.13)
76	9	23.2/5.4	74.5/5.6	Luciferin-binding protein	*Alexandrium catenella* ABY78836	Bioluminescence (02.45.01)
78	3	35.9/4.3	51.6/5.7	Methionine S-adenosyl transferase	*Euglena gracilis* ADH43284	Degradation of methionine (01.01.06.05.02)
12	2	28.0/4.7	38.0/9.1	Peridinin chlorophyll-a binding protein	*Symbiodinium* sp. AFH88375	Light absorption (02.45.03)
67	11	19.5/5.8	38.0/9.1	Peridinin chlorophyll-a binding protein	*Symbiodinium* sp. AFH8837[illegible]	Light absorption (02.45.03)
77	11	19.0/5.6	38.0/9.1	Peridinin chlorophyll-a binding protein	*Symbiodinium* AFH8[illegible]75	Light absorption (02.45.03)
81	9	19.6/7.2	38.0/9.1	Peridinin chlorophyll-a binding protein	*Symbiodinium* sp. AFH88375	Light absorption (02.45.03)
82	20	25.9/7.4	37.8/6.6	Peridinin-chlorophyll a-binding protein	*Symbiodinium* sp [illegible]1874	Light absorption (02.45.03)
83	17	25.7/7.7	38.2/8.7	Peridinin-chlorophyll a-binding protein	*Amphidinium carterae* P80484	Light absorption (02.45.03)
84	17	26.4/8.4	37.8/6.6	Peridinin-chlorophyll a-binding protein	*Symbiodinium sp.* P51874	Light absorption (02.45.03)
100	17	24.6/6.4	38.0/9.1	Peridinin chlorophyll-a binding protein	*Symbiodinium* sp. AFH88375	Light absorption (02.45.03)
101	14	26.4/7.1	38.0/9.1	Peridinin chlorophyll-a binding protein	*Symbiodinium* sp. AFH88375	Light absorption (02.45.03)
102	7	26.4/7.3	38.0/9.1	Peridinin-chlorophyll a-binding protein	*Symbiodinium* sp. AFH88375	Light absorption (02.45.03)
103	20	25.8/7.3	38.0/9.1	Peridinin chlorophyll-a binding protein	*Symbiodinium* sp. AFH88375	Light absorption (02.45.03)
105	14	19.1/8.2	38.0/9.1	Peridinin chlorophyll-a binding protein	*Symbiodinium* sp. AFH88375	Light absorption (02.45.03)
106	9	19.8/7.6	38.0/9.1	Peridinin chlorophyll-a binding protein	*Symbiodinium* sp. AFH88375	Light absorption (02.45.03)
107	10	19.8/8.2	38.0/9.1	Peridinin chlorophyll-a binding protein	*Symbiodinium* sp. AFH88375	Light absorption (02.45.03)
109	18	25.6/8.1	38.9/9.0	Peridinin-chlorophyll a-binding protein	*Gonyaulax polyedra* O00941	Light absorption (02.45.03)
110	12	25.8/7.3	38.0/9.1	Peridinin chlorophyll-a binding protein	*Symbiodinium* sp. AFH88375	Light absorption (02.45.03)
133	7	24.6/7.0	38.0/9.1	Peridinin chlorophyll-a binding protein	*Alexandrium minutum* GW801171	Light absorption (02.45.03)
159	12	17.8/7.0	38.0/9.1	Peridinin chlorophyll-a binding protein	*Symbiodinium* sp. AFH88375	Light absorption (02.45.03)
19	6	44.3/5.0	109.4/6.0	Predicted protein	*Nematostella vectensis* EDO31815	Unclassified protein (99)
23	9	23.5/6.6	27.5/5.2	Proteasome subunit	*Perkinsus marinus* EER11732	Proteasomal degradation (14.13.01.01)
104	8	25.6/6.9	27.9/5.8	Proteasome subunit	*Alexandrium fundyense* A4UHA5	Proteasomal degradation (14.13.01.01)
108	4	25.8/7.8	27.9/5.8	Proteasome subunit	*Perkinsus marinus* XP_002764909	Proteasomal degradation (14.13.01.01)
132	4	19.9/6.0	22.6/6.1	Proteasome subunit	*Daphnia magna* JAN48661	Proteasomal degradation (14.13.01.01)
99	7	14.4/6.8	partial	Protein kinase C conserved region 2, partial	*Brassica napus*	Protein modification by phosphorylation (14.04.03)
131	13	19.5/5.6	33.2/5.9	Ribose-5-phosphate isomerase	*Heterocapsa triquetra* Q5ENN9	Pentose phosphate pathway (02.07)
46	25	39.9/6.0	59.5/5.4	Ribulose bisphosphate carboxylase	*Gonyaulax polyedra* Q42813	Photosynthesis (02.30)
90	16	19.5/6.9	79.1/5.8	Ribulose bisphosphate carboxylase	*Heterocapsa triquetra* Q5ENN5	Photosynthesis (02.30)
25	7	16.1/5.4	132.0/6.6	Serine/threonine-protein phosphatase	*Symbiodinium microadriaticum* OLP947091	Protein modification by phosphorylation (14.04.03)
64	2	29.7/5.5	35.2/4.9	Serine/threonine-protein phosphatase	*Phytophthora parasitica* XP0089035861	Protein modification by phosphorylation (14.04.03)
17	3	32.4/4.8	16.7/6.1	Translation initiation inhibitor	*Perkinsus marinus* XP002786607	Translational control (12.07)

Table 1: Liquid chromatography-tandem mass spectrometry (LC-MS/MS) identification of the proteins with modified expression in the soluble proteome of the *Alexandrium pacificum* SG C10-3 strain exposed to metal stress (copper, lead, zinc, cadmium or polymetallic cocktail, at 6 µM).

Table 2: Liquid chromatography-tandem mass spectrometry (LC-MS/MS) identification of the proteins with modified expression in the soluble proteome of the *Alexandrium pacificum* TAR C5-4F strain exposed to metal stress (copper, lead, zinc, cadmium or polymetallic cocktail, at 6 µM).

Figure 1: Location of the sampling stations. (**A**) Sampling station for the *Alexandrium pacificum* SG C10-3 strain (**B**) Sampling station for the *A. pacificum* TAR C5-4F strain.

Figure 2: Schematic representation of the experimental procedure. (**A**) *Alexandrium pacificum* cells (strains SG and TAR; see Figure 1) were grown with (M^{2+}) or without metals (control) (**B**) Intracellular paralytic shellfish toxin (PST) contents were measured (**C**) After extraction, membrane proteins were separated by 2-D electrophoresis. Proteins (spots) of interest were picked to be identified by liquid chromatography-tandem mass spectrometry (LC-MS/MS). Protein names/functions were determined with Uniprot/NCBI database queries.

Figure 3: Representative 2-D maps comparing the soluble proteomes of the *Alexandrium pacificum* SG C10-3, obtained in control and metal-contaminated conditions. (**A**) Protein expression profiles of the *Alexandrium pacificum* SG C10-3 grown in control or metal-contaminated conditions (copper, lead, zinc, cadmium or polymetallic cocktail, at 6 µM). Proteins are identified by their spot numbers (**B**) Names of the proteins with modified expression (proteins of interest) on 2-D maps are shown with their fold differences; in black: upregulated proteins; in grey: downregulated proteins; A: appeared proteins; D: disappeared proteins. *, ** and ***: proteins with expression nearly significantly*, significantly** and very significantly*** different under metal stress, with: $0.05 < P^{*} \leq 0.10$; $0.01 < P^{**} \leq 0.05$; and $P^{***} \leq 0.01$, respectively.

Figure 4: Biological functions assigned to the proteins with modified expression (proteins of interest) in the soluble proteome of the *Alexandrium pacificum* SG C10-3

strain exposed to metal stress (copper, lead, zinc, cadmium or polymetallic cocktail, at 6 µM).

Figure 5: Representative 2-D maps comparing the soluble proteomes of *Alexandrium pacificum* TAR C5-4F obtained in control and metal-contaminated conditions. (**A**) Protein expression profiles of the *Alexandrium pacificum* TAR C5-4F strain grown in control or metal-contaminated conditions (copper, lead, zinc, cadmium or polymetallic cocktail, at 6 µM). Proteins are identified by their spot numbers (**B**) Names of the proteins with modified expression (proteins of interest) on 2-D maps are shown with their fold; in black: upregulated proteins; in grey: downregulated proteins; A: appeared proteins, D: disappeared proteins. *, ** and ***: proteins with expression nearly significantly*, significantly** and very significantly*** different under metal stress, with: $0.05 < P^{*} \leq 0.10$; $0.01 < P^{**} \leq 0.05$; and $P^{***} \leq 0.01$, respectively.

Figure 6: Biological functions assigned to the proteins with modified expression (proteins of interest) in the soluble proteome of the *Alexandrium pacificum* TAR C5-4F strain exposed to metal stress (copper, lead, zinc, cadmium or polymetallic cocktail, at 6 µM).

Figure 7: Venn diagrams showing the numbers of appeared, upregulated, downregulated, or disappeared proteins (proteins of interest), expressed in common in the *Alexandrium pacificum* SG C10-3 and TAR C5-4F strains grown in metal-contaminated conditions (copper, lead, zinc, cadmium or polymetallic cocktail, at 6 µM). *: names of the differentially expressed proteins in common between the two strains.

Figure 8: Proportions (in %) of the different toxin contents (GTX4, GTX1, GTX5, GTX3, GTX2, neo-STX, C1 and C2) in the cells of the *Alexandrium pacificum* SG C10-3 (SG) and TAR C5-4F (TAR) strains grown in control or in metal-contaminated conditions (copper, lead, zinc, cadmium or polymetallic cocktail, at 6 µM).

Figure 9: Histograms showing the different toxin contents (total, GTX4, GTX1, GTX5, GTX3, GTX2, neo-STX, C1 and C2) in the cells of the *Alexandrium pacificum* SG C10-3

(SG) and TAR C5-4F (TAR) strains grown in control or in metal-contaminated conditions (copper, lead, zinc, cadmium or polymetallic cocktail, at 6 µM). **: toxin contents significantly different to control conditions, with: $0.01 < P^{**} \leq 0.05$. ▲▲: toxin contents significantly higher in SG C10-3 than in TAR C5-4F with: $0.01 < P^{**} \leq 0.05$; ▲▲▲ : toxin contents significantly higher in SG C10-3 than in TAR C5-4F with: $P^{***} \leq 0.01$.

CREDIT AUTHORS STATEMENT

Natacha Jean: Proteomics experiments, toxin and proteomics data treatment, writing the paper.

Luce Perié: Proteomics experiments and data treatment.

Estelle Dumont: Proteomics experiments and data treatment.

Lucie Bertheau: Proteomics experiments and data treatment.

Thierry Balliau : Protein identification by liquid chromatography-tandem mass spectrometry.

Amandine M.N. Caruana: Toxin analysis and contributor to paper writing.

Zouher Amzil : Toxin analysis and contribution to paper writing.

Mohamed Laabir: Cell cultures and contribution to paper writing.

Estelle Masseret: Cell cultures, writing the paper.

Declaration of interests

☒ The authors declare that they have no known competing financial interests or personal relationships that could have appeared to influence the work reported in this paper.

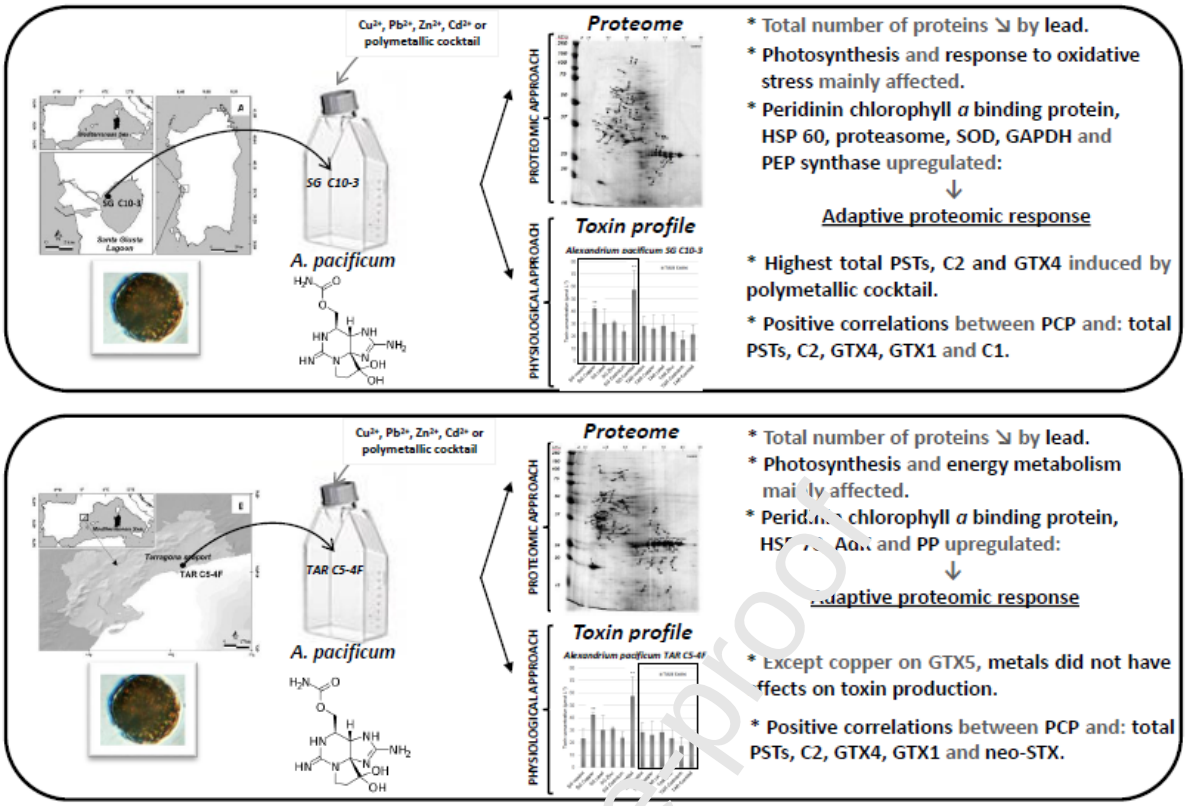

Graphical abstract

Highlights

- Metals modify soluble proteomes and toxin profiles in the *A. pacificum* strains.
- Downregulation of photosynthesis proteins was observed in the *A. pacificum* strains exposed to metals.
- Adaptive proteomic response exist in the *A. pacificum* strains under metal stress conditions.
- SG C10-3 strain upregulates more proteins than TAR C5-4F strain, revealing proteomic variability between the two strains exposed to metals.
- Polymetallic cocktail and copper have significant effects on the PST contents in the SG C10-3 strain.
- PST showed correlations with PCP in both strains: photosynthesis may be positively related to toxin production.